

1 **An assessment of CO₂ storage and sea-air fluxes for the Atlantic Ocean and**
2 **Mediterranean Sea between 1985 and 2018.**

3 **Fiz F. Perez¹, M. Becker², N. Goris³, M. Gehlen⁴, M. Lopez-Mozos¹, J. Tjiputra³, A. Olsen²,**
4 **J.D. Müller⁵, I. E. Huertas⁶, T. T. T. Chau⁴, V. Cainzos⁷, A. Velo¹, G. Benard⁴, J. Hauck⁸,**
5 **N. Gruber⁵ and Rik Wanninkhof⁹.**

6 ¹Instituto de Investigaciones Marinas (IIM), CSIC, Vigo, Spain..

7 ²Geophysical Institute, University of Bergen, and Bjerknes Centre for Climate Research, Bergen,
8 Norway

9 ³NORCE Climate & Environment, Bjerknes Centre for Climate Research, Bergen, Norway

10 ⁴Laboratoire des Sciences du Climat et de l'Environnement, LSCE/IPSL, CEA-CNRS-UVSQ,
11 Université, Paris-Saclay, F-91191 Gif-sur-Yvette, France

12 ⁵Environmental Physics, Institute of Biogeochemistry and Pollutant Dynamics, ETH Zurich,
13 Zürich, Switzerland.

14 ⁶Instituto de Ciencias Marinas de Andalucía (ICMAN-CSIC), Puerto Real, Cadiz, Spain.

15 ⁷Unidad Océano y Clima, Instituto de Oceanografía y Cambio Global, IOCAG, Universidad de
16 Las Palmas de Gran Canaria, ULPGC, Unidad Asociada ULPGC-CSIC, Canary Islands, Spain.

17 ⁸Alfred-Wegener-Institut, Helmholtz-Zentrum für Polar- und Meeresforschung, Bremerhaven,
18 Germany

19 ⁹Atlantic Oceanographic and Meteorological Laboratory, National Oceanic and Atmospheric
20 Administration, Miami, Florida, USA

21 Corresponding author: Fiz F. Perez (fiz.perez@iim.csic.es)

22
23 **Key Points:**

- 24 • From 1985 to 2018, pCO₂ products suggest a slightly lower mean CO₂ uptake (-
25 0.37±0.06 PgC yr⁻¹) than ocean models (0.47±0.15 PgC yr⁻¹)
- 26 • Since 2000, the CO₂ uptake is increasing twice as fast in the pCO₂ products compared to
27 the models.
- 28 • Major differences between models and pCO₂ products are attributed to the outgassing of
29 riverine carbon and the seasonal cycle of pCO₂.
30

31 **Abstract**

32 As part of the second phase of the Regional Carbon Cycle Assessment and Processes
33 project (RECCAP2), we present an assessment of the carbon cycle of the Atlantic Ocean, including
34 the Mediterranean Sea, between 1985 and 2018 using global ocean biogeochemical models
35 (GOBMs) and estimates based on surface ocean partial pressure of CO₂ (pCO₂ products) and ocean
36 interior dissolved inorganic carbon observations. Estimates of the Atlantic Ocean long-term mean
37 net annual CO₂ uptake based on GOBMs and pCO₂ products are in reasonable agreement (-
38 0.47±0.15 PgCyr⁻¹ and -0.37±0.06 PgCyr⁻¹, respectively), with the higher uptake in the GOBM-
39 based estimates likely being a consequence of a deficit in the representation of natural outgassing
40 of land derived carbon. In the GOBMs, the CO₂ uptake is increasing with time at rates close to
41 what one would expect from the atmospheric CO₂ increase, but pCO₂ products estimate a rate
42 twice as fast. The largest disagreement in the CO₂ flux between GOBMs and pCO₂ products is
43 found north of 50°N, coinciding with the largest disagreement in seasonal cycle and interannual
44 variability. The rate of accumulation of anthropogenic CO₂ (C_{ant}) over 1994-2007 in the Atlantic
45 Ocean is 0.52±0.11 PgC yr⁻¹ according to the GOBMs, 28±20% lower than that derived from
46 observations. Around 70% of this accumulated C_{ant} is taken up from the atmosphere, while the
47 remainder is imported from the Southern Ocean through lateral transport.

48 **Plain Language Summary**

49 This study contributes to the second Regional Carbon Cycle Assessment and Processes by
50 presenting a carbon cycle evaluation of the Atlantic Ocean including the Mediterranean Sea
51 between 1985 and 2018. The assessment draws on output from global ocean biogeochemical
52 models along with estimates based on observations of surface ocean partial pressure of CO₂ (pCO₂
53 products) and ocean interior dissolved inorganic carbon. The models suggest that the Atlantic took
54 up -0.47±0.15 Pg of carbon per year, in reasonable agreement with an uptake of -0.37±0.06 Pg
55 carbon per year computed from pCO₂ products. In the models, the rate of CO₂ uptake is keeping
56 pace with the increase of atmospheric CO₂, but it is twice as fast in the pCO₂ products. Most of
57 the uptake of CO₂ by the ocean occurs in response to excess CO₂ released to the atmosphere from
58 human activities. The so-called anthropogenic carbon accumulates in the Atlantic Ocean at a rate
59 of 0.52±0.11 Pg carbon per year according to the models. This estimate is 28±20% lower than that
60 derived from observations. Further investigation reveals that about 70% of the accumulated
61 anthropogenic carbon is taken up from the atmosphere, while the remainder is imported from the
62 Southern Ocean.

63

64 **1 Introduction**

65 During the International Geophysical Year 1957-58, Taro Takahashi (1930-2019) made
66 the first systematic and accurate measurements of carbon dioxide gas (CO₂) partial pressure in the
67 air and sea surface along an Atlantic Ocean transect from Greenland to Cape Town (Takahashi,
68 1961). Since these early times, the importance of monitoring seawater CO₂ partial pressure (pCO₂)

69 for the assessment of air-sea exchanges of CO₂ has been increasingly recognized. Today,
70 measurements of pCO₂ have become an integral part of ocean monitoring programs including
71 Eulerian time series stations (Bates et al. 2014), oceanographic buoy arrays, and Ships of
72 Opportunity (SOOP) programs (Pfeil et al. 2013; Sabine et al. 2013; Bakker et al. 2016;
73 Wanninkhoff et al. 2019). Early measurements of pCO₂ highlighted spatial patterns that were
74 confirmed later by time-series measurements (Keeling, 1993, Michaels et al., 1994, Bates et al.,
75 1998, Gruber et al., 1998), large-scale data compilations and the development of surface ocean
76 CO₂ climatologies (Takahashi et al. 2002, Takahashi et al. 2009). The North Atlantic between
77 25°N and 76°N stands out as a region of intense CO₂ uptake by the ocean. It represents only 7%
78 of the ocean surface, but accounts for 23% of the global uptake (Takahashi et al. 2009; Schuster
79 et al. 2013). Approximately two thirds of its contemporary uptake is caused by natural processes,
80 such as heat loss and export production, while the remaining one third is caused by the increasing
81 concentrations of CO₂ in the atmosphere and is therefore called uptake of anthropogenic carbon,
82 C_{ant} (Mikaloff-Fletcher et al 2007; Gruber et al. 2009; Keeling et al. 1995; Watson et al. 1995).
83 The local uptake of C_{ant} by sea-air exchange in the Atlantic combined with the net northward
84 transport of C_{ant}-rich southern latitude waters by the upper limb of the Atlantic meridional
85 overturning circulation (AMOC) (McDonald et al. 2003; Roson et al. 2003; Perez et al. 2013;
86 Brown et al. 2021) leads to a high accumulation of C_{ant} throughout the water column of the
87 Atlantic, accounting for approximately 35% of the global total storage (Sabine et al 2004; Gruber
88 et al. 2019). Earlier studies highlighted the role of the AMOC, a key component of the global ocean
89 circulation and a distinctive dynamic element of the Atlantic circulation, in the redistribution of
90 CO₂ (Holfort et al., 1998; Wallace 2001). The AMOC further links the upper ocean thermohaline
91 circulation with the intense Deep Western Boundary Current (DWBC) connecting the waters
92 formed in the subpolar North Atlantic with the Southern Ocean (Haine et al. 2016, Hirschi et al.
93 2020, Rhein et al. 2015). The DWBC contributes to natural interhemispheric carbon exchanges by
94 transporting between 0.5 and 1 PgC yr⁻¹ from North Atlantic uptake regions southward (Aumont
95 et al 2001; Macdonald et al. 2003; Resplandy et al 2018).

96 As part of the second phase of the Regional Carbon Cycle Assessment and Processes
97 project (RECCAP2), we complement these earlier studies about the Atlantic carbon budget with
98 an analysis of the latest observation- and model-based estimates of the Atlantic Ocean including
99 sea-air fluxes (natural and anthropogenic), storage, and transport of CO₂ for the years 1985 to
100 2018. Following Fay and McKinley (2014), RECCAP2 divides the Atlantic into five regions or
101 biomes (Figure 1a), namely the North Atlantic subpolar gyre (NA SPSS), the seasonally and
102 permanently stratified regions of the North Atlantic subtropical gyre (NA STSS and NA STPS),
103 the Atlantic equatorial upwelling region (AEQU), and the seasonally stratified South Atlantic
104 subtropical gyre to ~35°S (SA STPS). The Mediterranean Sea is also included as a single, sixth
105 biome (MED). Among these regions, the NA SPSS stands out as a biome with a high spatial and
106 temporal variability, which still challenges our understanding, assessments, and modeling efforts
107 despite the increase in observational capacity over the last two decades. During the RECCAP1
108 period (1990-2009), Schuster et al. (2013) estimated an average CO₂ uptake of -0.21 ± 0.06 PgC yr⁻¹

109 ¹ (*positive or negative sign indicating flux into the atmosphere or ocean, respectively*) between
110 49°N and 79°N, consistent across observation-based estimates and numerical models used. This
111 flux amounts to 10% of the global uptake and makes the NA subpolar region one of the regions
112 with the highest CO₂ uptake density. Understanding the seasonal, interannual and long-term
113 variability of the high latitude Atlantic CO₂ sink has been the focus of many observational and
114 modeling studies (e.g., Thomas et al., 2008; Ullman et al., 2009; Watson et al., 2009; Tjiputra et
115 al., 2012; Breeden and McKinley, 2016; Lesseure et al., 2020; Macovei et al., 2020). It has become
116 clear, that the variability of sea-air fluxes of CO₂ and C_{ant} storage rates in this region is influenced
117 by regional modes of climate variability, such as the North Atlantic Oscillation (NAO), through
118 its effect on wind patterns and ocean heat loss, mixing, and deep water formation. During the time
119 period from the 1990s to the 2000s, C_{ant} storage rates decreased in the subpolar NA in response to
120 the shift from predominantly high (1990-95) to low (2002 to 2007) NAO (Perez et al. 2008,
121 Steinfeldt et al. 2009, Perez et al. 2013; Gruber et al., 2019). Recent observations show a
122 reinvigoration of this storage associated with increased convection in the mid 2010s (Fröb et al.,
123 2016), as a consequence of a shift back to positive NAO conditions.

124 The subtropical North Atlantic (in RECCAP1 defined to be 18° to 49°N, 7.2% of the ocean
125 surface) was shown to be a CO₂ sink, with a net uptake of -0.26 ± 0.06 PgC yr⁻¹ between 1990 and
126 2009 (Schuster et al. 2013), due in approximately equal parts to C_{ant} and natural CO₂ uptake, where
127 the latter is driven mainly by net heat loss, with limited contributions from biological activity
128 (Gruber et al., 2009). The mean subtropical gyre uptake rate (-0.91 mol C m⁻² yr⁻¹) is similar to
129 that observed at the Bermuda Atlantic Time-series Study (Bates et al. 2014), even though the
130 eastern return branch of the subtropical gyre showed lower uptake values (Santana-Casiano et al.,
131 2007). At both sites, the interannual variability of CO₂ flux correlates with sea surface temperature
132 and mixed layer depth anomalies (González-Dávila et al., 2010; Gruber et al., 2002; Santana-
133 Casiano et al., 2007). SST is the main driver of the seasonal cycle in the subtropics, driving an
134 outgassing of CO₂ in summer and uptake in winter.

135 The tropical Atlantic is the second largest oceanic source of CO₂ to the atmosphere, after
136 the tropical Pacific, with an annual emission of 0.10-0.11 PgC yr⁻¹ (Takahashi et al., 2009;
137 Landschützer et al., 2014) due to frequent upwelling of cold, CO₂-rich water in the eastern parts.
138 Based on six different methodologies, the RECCAP1 estimate for this regions converged on an
139 outgassing of 0.12 ± 0.04 PgC yr⁻¹ between 1990 and 2009 (Schuster et al., 2013). The increase in
140 atmospheric CO₂ has decreased the outgassing since preindustrial times, as the ocean
141 supersaturation is reduced by about 50% (Gruber et al., 2009). This implies an uptake of
142 anthropogenic CO₂. Gruber et al. (2009) also suggested that an important part of this natural
143 outgassing is due to the riverine contribution of organic matter, especially that stemming from the
144 Amazon river (Louchard et al., 2021).

145 The subtropical South Atlantic is a sink for atmospheric CO₂ (Schuster et al., 2013;
146 Rödenbeck et al., 2015), driven in almost equal parts by natural and anthropogenic CO₂ fluxes
147 (Gruber et al., 2009). It has been suggested that strong upwelling events in the eastern part generate

148 significant interannual variability (Schuster et al., 2013). However, pCO₂ variability in the SA
149 STPS biome as shown by Rodenbeck et al. (2015) is relatively low. From 1990 to 2009, this region
150 was a CO₂ sink of -0.14 ± 0.04 PgC yr⁻¹ on average, combining areas with a net outgassing north of
151 the 23°C isotherm (Ito et al., 2005) with areas of absorption to the south. This region is relatively
152 poorly sampled with the domain north of 31°S acting as a source in spring and sink in autumn
153 (Santana-Casiano et al., 2007; González-Dávila et al., 2009; Padín et al., 2010). Estimates of long-
154 term CO₂ flux trends in this region are highly dependent on the methodology used (Schuster et al.,
155 2013).

156 The Mediterranean Sea represents 3.5% of the Atlantic Ocean area and is the only mid-
157 latitude ocean basin in which deep convection occurs (see Suppl-Info Text 1). This circulation is
158 responsible for a relatively large inventory of C_{ant} of 1.7 PgC as estimated from CFCs (Schneider
159 et al., 2010). The overturning time is very fast in relation to that of the global ocean (60 to 220
160 years vs more than 1000 years; Stöven and Tanhua, 2014; Khatiwala et al., 2013) and allows a
161 complete renewal of water in the basin on a relatively short time scale. Hence, surface waters
162 enriched in C_{ant} transfer this signature to deep layers relatively quickly, leading to all water masses
163 in the basin being already invaded by C_{ant} (Hassoun et al., 2015). However, surface pCO₂ exhibits
164 large variability, due to the large heterogeneity of physical and trophic regimes in the two main
165 Mediterranean sub-basins, with a marked west-to-east oligotrophy gradient and different
166 atmospheric forcings that regulate seawater pCO₂ and the air-sea CO₂ exchanges (Krasakopoulos
167 et al., 2009; 2017, Ingrosso et al., 2016, Urbini et al., 2020, De Carlo et al., 2013; Kapsenberg et
168 al., 2017, Petihakis et al., 2018, Sisma-Ventura et al., 2017, Coppola et al., 2018, Wimart-Rousseau
169 et al., 2021).

170 In RECCAP1, the assessment of the ocean carbon cycle relied on five global ocean
171 biogeochemical models (GOBMs), several atmospheric and oceanic inversions, the pCO₂
172 climatology published by Takahashi et al (2009), as well as the SOCAT (Surface Ocean CO₂ Atlas)
173 database. A crucial progress since RECCAP1 are annual updates of SOCAT (Bakker et al., 2016),
174 with over 33.7 million quality-controlled surface ocean pCO₂ measurements in the 2022 release
175 (Bakker et al., 2022). The availability of these data sparked the development of time-varying
176 reconstructions of surface ocean pCO₂ distributions. These pCO₂ products rely on advanced
177 statistical techniques and neural networks to extrapolate sparse observations in time and space to
178 achieve temporally resolved global coverage (e.g., Landschützer et al, 2014, Rödenbeck et al.,
179 2014, Gregor et al., 2019, Chau et al., 2022). Similarly, advances in biogeochemical modeling led
180 to the contribution of an increased number of GOBMs to RECCAP2 that provided output from up
181 to four different simulations allowing to disentangle the natural carbon cycle and the anthropogenic
182 perturbation (Wanninkhof et al., 2013, Friedlingstein et al., 2022).

183 Improved process understanding and increasing availability of ocean biogeochemical data
184 have led to advances in GOBMs, particularly in simulating the large-scale features and mean state
185 of the ocean carbon cycle (Seferian et al., 2020). When forced with atmospheric reanalysis and
186 atmospheric CO₂ concentration data, these models were assessed to be suitable in quantifying the

187 global ocean carbon fluxes, from annual mean to interannual time-scale (Hauck et al., 2020).
188 Regionally, such models have also been shown to be capable of simulating the observed long-term
189 pCO₂ trends (Tjiputra et al., 2014). Nevertheless, some GOBMs still have difficulties in
190 representing the observed seasonal cycle in key ocean sink regions in the North Atlantic, likely
191 owing to mismatch in the timing of deep winter mixing and/or biological bloom events (Tjiputra
192 et al., 2012; Schwinger et al., 2016). Since RECCAP1, the number of ocean biogeochemical
193 models has increased, and while not all RECCAP1 models participated in the RECCAP2 exercise,
194 those that do have likely gone through iterations of improvements (the readers are referred to
195 Supplementary Table S1 in DeVries et al., in review, for individual biogeochemical model
196 description). In the Atlantic domain, recent developments in the ocean physical component have
197 led to better representation of large scale circulation and ventilation processes (Hirschi et al. 2020),
198 which could have strong implications on the transports of biogeochemical tracers driving the sea-
199 air CO₂ fluxes and interior carbon sequestration in this basin.

200 This synthesis paper is structured as follows. Section 2 provides the details of the database
201 consisting of data sets based on observations of both surface pCO₂ and the marine carbonate
202 system in the ocean interior, and an ensemble of global biogeochemical models together with a
203 regional model and an assimilation model. In Section 3, the CO₂ fluxes obtained for each class of
204 products are described and analyzed considering both the mean values for the study period, trends
205 in two periods (1985-2000 and 2000-2018), the seasonal cycle and the interannual variability of
206 CO₂ fluxes. In addition, the accumulation of anthropogenic CO₂ in the ocean interior is evaluated.
207 In section 4, we discuss the results obtained in RECCAP2 in comparison to RECCAP1, as well as
208 the consistency and discrepancies between the global biogeochemical models and different data
209 products, and suggest ways for future improvements. Section 5 summarizes the main conclusions
210 and lists some of the remaining challenges to be solved in future versions of RECCAP.

211 **2 Methods**

212 The Atlantic Ocean and its subdivision into biomes is defined by the RECCAP2 basin mask
213 (<https://reccap2-ocean.github.io/>, last access: 2022/10/25) and extends from approximately 79°N
214 to approximately 35°S (Figure 1). The RECCAP2 ocean database used in this study is described
215 in DeVries et al. (in review) and contains two types of products: 1) Observation-based products
216 for surface ocean pCO₂ (pCO₂ products) and for ocean interior C_{ant} reconstruction and, 2) Global
217 and Regional Ocean Biogeochemical Model (GOBM/ROBM) hindcast simulations and an ocean
218 data-assimilation model. All products have been re-gridded onto a common 1°×1° horizontal grid
219 by the data providers. Ocean model outputs were either provided on the models' standard depth
220 levels or regrided to fixed depth levels chosen by the data providers.

221 2.1. Observation-based products

222 2.1.1 pCO₂ products

223 This analysis draws on a variety of observation-based products for surface ocean pCO₂ and
224 sea-air CO₂ fluxes (Table S1). These products are based on the interpolation of in situ pCO₂ data
225 compiled within SOCAT (Bakker et al., 2016; <https://doi.org/10.25921/1h9f-nb73>) to near-global

226 coverage of monthly surface ocean $p\text{CO}_2$ distributions at 1° horizontal resolution. Several
 227 interpolation methods are used including machine learning techniques (Landschützer et al., 2014;
 228 Gregor et al., 2019; Watson et al., 2020; Chau et al., 2022; Gloege et al. 2021; Gregor and Gruber,
 229 2021; Iida et al., 2021, Zeng et al., 2022) and a diagnostic mixed layer scheme (Rödenbeck et al.,
 230 2013). Sea-air CO_2 fluxes (FCO_2) are computed from reconstructed $p\text{CO}_2$ fields following:

$$231 \quad \text{FCO}_2 = K_w (1-f_{\text{ice}}) K_0 (p\text{CO}_2 - p\text{CO}_{2,\text{air}})$$

232 where: K_w is monthly averaged gas transfer velocity; f_{ice} is sea-ice cover fraction; K_0 is CO_2
 233 solubility in seawater; and $p\text{CO}_2$, and $p\text{CO}_{2,\text{air}}$ are the partial pressures of CO_2 in seawater
 234 (nominally at 5 m depth) and in the overlying atmosphere (nominally at 10 m height), respectively.
 235 The gas transfer velocity is computed as a function of wind speed at 10 m mostly assuming a
 236 quadratic relationship (Wanninkhof, 1992; 2014, Ho et al. 2006). Positive values of FCO_2 mean
 237 outgassing from the sea to the atmosphere. For the set of $p\text{CO}_2$ products, the uncertainty of the
 238 mean is determined as the standard deviation of the FCO_2 of the nine $p\text{CO}_2$ products referenced in
 239 Table S1.

240 The $p\text{CO}_2$ product by Watson et al. (2020), UOEX-Wat20, is fundamentally different from
 241 the other products as it adjusts the underlying $p\text{CO}_2$ observations for near-surface temperature
 242 gradients following Goddijn-Murphy et al. (2015) and Woolf et al. (2016), henceforth referred to
 243 as the surface skin effects. While UOEX-Wat20 is included in the analysis, it is kept distinct from
 244 the other nine $p\text{CO}_2$ products, because of the difference in approach.

245

246 *2.1.2 Ocean interior C_{ant} reconstructions*

247 Furthermore, we consider two ocean interior observation-based products, one based on
 248 measurements of dissolved inorganic carbon (DIC) concentrations collected over more than 30
 249 years, and other physical and biogeochemical parameters by Gruber et al. (2019), and another one
 250 combining an inversion approach with tracer measurements by Khatiwala et al. (2009). The Gruber
 251 et al. (2019) product provides an estimate of the ocean C_{ant} storage change between the years 1994
 252 and 2007. This estimate is based on the eMLR(C^*) method (Clement and Gruber, 2018) applied
 253 on the GLODAPv2 data (Olsen et al., 2016). It includes both the steady-state and non-steady-state
 254 components of the C_{ant} accumulation in the ocean interior. The product from Khatiwala et al.
 255 (2009) provides estimates of the ocean C_{ant} content from 1850 up to 2011 and is based on a Green's
 256 Function approach that allows a gradual increase in the CO_2 disequilibrium between the
 257 atmosphere and the ocean. This estimate considers the steady-state increase in C_{ant} only. Note that
 258 only the ΔC_{ant} reconstruction product from Gruber et al. (2019) is included in the RECCAP2 ocean
 259 database. In the North Atlantic and below 3000 m, Gruber et al. (2019) estimated a C_{ant}
 260 accumulation of 0.05 PgC/yr (~8% of the accumulation above 3000m), which has been
 261 proportionally distributed in the biomes considering the GOBMs` C_{ant} accumulation below 3000
 262 m.

263 The C_{ant} reconstruction product from Khatiwala et al. (2009) was pre-processed to match
264 the RECCAP2 $1^\circ \times 1^\circ$ grid and coincide with the vertical discretization of the ΔC_{ant} reconstruction
265 product from Gruber et al. (2019). Since the product provides annual values, we calculated the
266 anthropogenic carbon rate of change (ΔC_{ant}) between 1994-2007 to allow comparison with Gruber
267 et al. (2019). The ΔC_{ant} reconstruction-product of Gruber et al. (2019) does not cover the entire
268 NA SPSS biome explored in our study, so we extrapolated the product to the Nordic Seas assuming
269 the same vertical ΔC_{ant} profile as at 65°N , resulting in a 23% increase of C_{ant} storage rate in the
270 NA SPSS biome. The percentage of increase obtained was applied to Khatiwala et al. (2009), as it
271 also does not fully cover the NA SPSS biome. The uncertainty in C_{ant} storage rate in each biome
272 was estimated by surface scaling of the uncertainties of the North and South Atlantic provided by
273 Gruber et al. (2019). For the Khatiwala et al. (2009) product a relative uncertainty of 17% was set
274 following Khatiwala et al., (2013).

275 2.2 Global ocean biogeochemical models

276 As an improvement from RECCAP1 (Wanninkhof et al., 2013), the RECCAP2 protocol
277 provides a set-up of four simulations with four combinations of atmospheric physical and CO_2
278 concentration forcings such that the simulated total CO_2 -fluxes can be divided into its steady-state
279 and non-steady state natural and anthropogenic components: (i) Simulation A: temporally varying
280 atmospheric reanalysis forcing and increasing atmospheric CO_2 , (ii) Simulation B: climatological
281 atmospheric forcing and constant pre-industrial atmospheric CO_2 , (iii) Simulation C:
282 climatological atmospheric forcing and increasing atmospheric CO_2 , and (iv) Simulation D:
283 temporally varying atmospheric reanalysis and constant preindustrial CO_2 .

284 We used outputs from 11 GOBMs of which the majority also contributes to the Global
285 Carbon Budget (Friedlingstein et al., 2020; Supplementary Table S2). All GOBMs used here are
286 general ocean circulation models with coupled ocean biogeochemistry, run in hindcast mode and
287 hence forced by atmospheric data sets. Details of the respective model resolutions, forcings, and
288 references are provided in an overview table in DeVries et al. (in review). All models performed
289 four simulations (A, B, C, and D), except for MOM6-Princeton (not C and D). Additionally, we
290 considered the output from the regional ocean biogeochemical model (ROBM) ROMS-
291 AtlanticOcean-ETHZ (Louchard et al., 2021) that only performed Simulation A. We also included
292 results from the ocean data-assimilation model OCIMv2021 (DeVries et al., 2022) that performed
293 simulations A, B and C. OCIMv2021 uses a climatological mean circulation but has time-varying
294 SST. It includes an abiotic carbon cycle model forced with atmospheric CO_2 to estimate the
295 anthropogenic carbon distribution.

296 To determine the FCO_2 for the period 1985-2018, for each GOBM and each biome, we
297 subtracted the linear trend of the respective fluxes estimated in Simulation B from Simulation A,
298 to correct for potential model-dependent drift. For the ensemble of GOBMs, the uncertainty of the
299 mean was determined as the standard deviation of the 11 models referenced in Table S2. For single
300 products, such as the ROBM and OCIMv2021, it was estimated as the standard deviation of the
301 annual mean FCO_2 values.

302 In order to be consistent with the ΔC_{ant} reconstruction product of Gruber et al. (2019), the
303 C_{ant} accumulation rate in the GOBMs was evaluated between 1994-2007. Therefore, C_{ant} was
304 calculated as the difference in DIC between the simulation with increasing atmospheric CO_2
305 concentrations (Simulation A) and the one with constant pre-industrial atmospheric CO_2
306 concentrations (Simulation D), both with time varying atmospheric physical forcing. We
307 considered all GOBMs that ran Simulation A and Simulation D (Supplementary Table S2).
308 However, MPIOM-HAMOCC was excluded from final analysis because of its large negative C_{ant}
309 values in the interior due to the inconsistent set-ups between its Simulations A and D. For the
310 OCIMv2021 model C_{ant} was determined as the difference between Simulations C (increasing
311 atmospheric CO_2 , climatological atmospheric forcing) and B (constant pre-industrial atmospheric
312 CO_2 , climatological atmospheric forcing), as this model uses a steady-state circulation and did not
313 run Simulations D. Once we obtained the total C_{ant} concentrations from all GOBMs products, we
314 computed the C_{ant} storage changes as the difference between the concentrations in 1994 and 2007.
315 C_{ant} concentration changes were vertically integrated to get the column inventory storage changes,
316 as well as biome-integrated C_{ant} accumulation rates. For the GOMBs ensemble, the uncertainty of
317 the mean C_{ant} accumulation rate is determined as the standard deviation of the C_{ant} accumulation
318 rates of the nine models referenced in Table S2.

319 2.3. Area Coverage

320 Practically all $p\text{CO}_2$ products considered have a spatial coverage of almost 100% of the Atlantic
321 basin, except JMA-MLR and MPI-SOMFFN with about 91-92% of area coverage. Here, $p\text{CO}_2$ -
322 product fluxes were not scaled to the same ocean area, following the assumption of Hauck et al.
323 (submitted), that the discrepancy arising from differences in covered area are smaller than the
324 uncertainty arising from any extrapolation to an equal area. All GOBMs cover more than 98% of
325 the area, except MPIOM-HAMOCC (95%) and CESM-ETHZ (97%). ROMS-ETHZ (ROBM)
326 covers 95% of the Atlantic Region, and only 93% of the NA SPSS biome and 25% of the
327 Mediterranean Sea. Likewise, most of the missing coverage of the MPIOM-HAMOCC is located
328 in the Mediterranean Sea, thus ROMS-ETHZ and MPIOM-HAMOCC have not been used for the
329 evaluation of the MED biome.

330 2.4 Riverine carbon outgassing

331 The flux of natural CO_2 across the air-sea interface includes also a flux balancing the input
332 of inorganic and organic carbon at the land-sea interface minus the fraction buried in marine
333 sediments (Regnier et al., 2012, Sarmiento and Sunquist, 1992). We refer to this flux component
334 as preindustrial riverine CO_2 outgassing (RCO). Since $p\text{CO}_2$ products are based on real-world
335 observations, they provide estimates of total FCO_2 , including the RCO. In contrast, RCO is not at
336 all or not adequately represented in GOBMs. Its approximation would require several thousands
337 of years of integration with a GOBM including a sediment module. None of the GOBMs used here
338 includes such a long pre-industrial spin-up (Terhaar et al., submitted). Though several of the
339 GOBMs analyzed in this study include river inputs of carbon, not all processes relevant for the
340 land-sea flux are adequately represented. In consequence, the average of the global imbalance

341 between river input and flux to the sediment is small ($<0.14 \text{ PgC yr}^{-1}$) in the GOBMs ensemble
342 (Terhaar et al., submitted) compared to the observation-based estimate of RCO recommended in
343 the RECCAP2 protocol, that amounts to $0.65 \pm 0.3 \text{ PgC yr}^{-1}$ (Regnier et al., 2022). Combining the
344 spatial distribution of RCO by Lacroix et al. (2020) and the globally integrated estimate by Regnier
345 et al. (2022) allows us, in principle, to estimate its contribution to FCO_2 at biome scale, albeit with
346 a large uncertainty and without considering the already present land-sea fluxes of the GOBMs.
347 However, the magnitude of RCO is a major source of uncertainty and hinders the straightforward
348 comparison of fluxes from pCO_2 products and GOBMs. Following RECCAP2 protocols, the RCO
349 adjustment of modeled FCO_2 is only assessed at biome and basin scale. About 40% of the global
350 estimated RCO occurs in the Atlantic Ocean with a particularly very large share in the NA STPS
351 biome (Table S3).

352 **3 Results**

353 3.1 Sea-air CO_2 fluxes

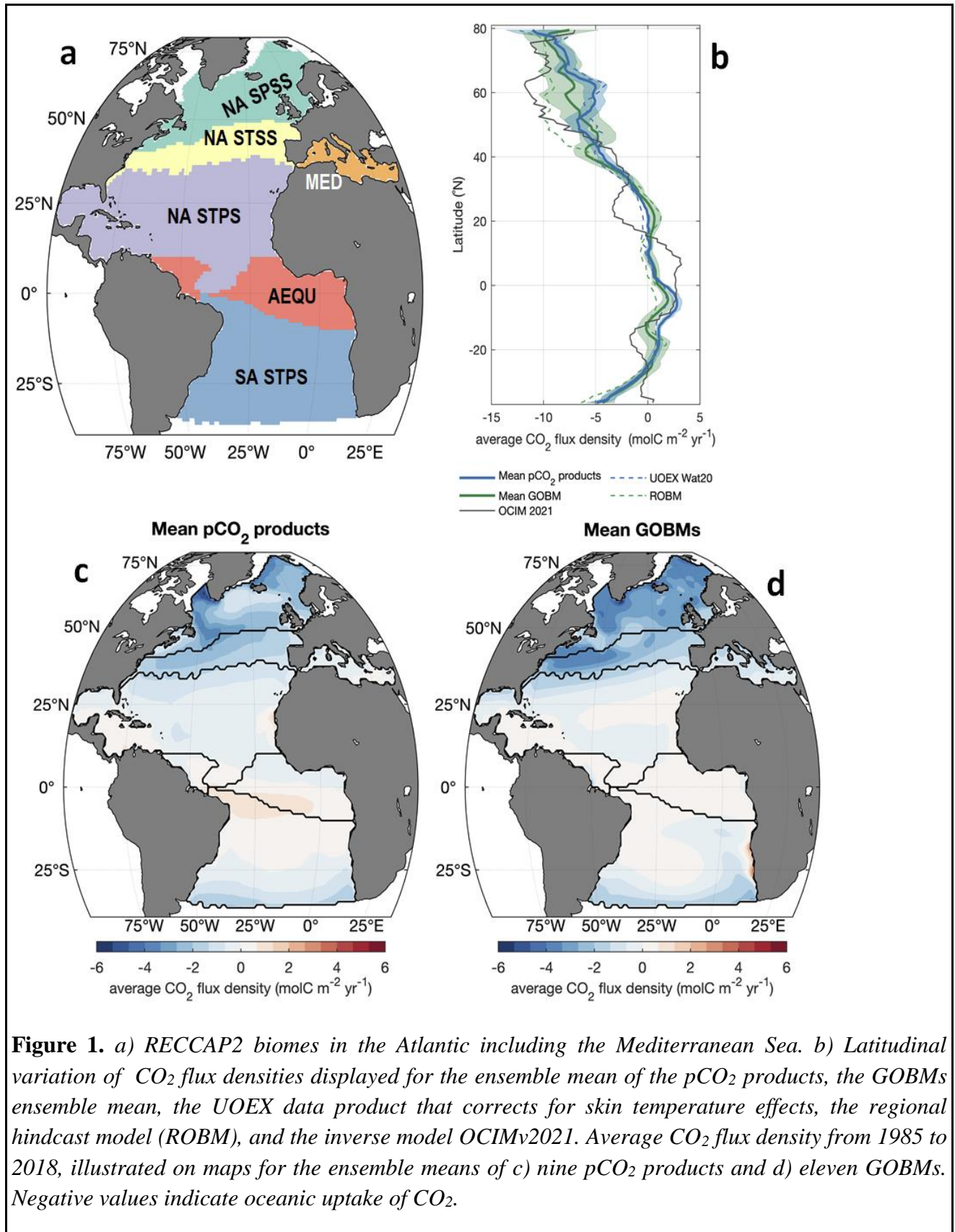
354 3.1.1 Long-term mean fluxes from 1985 to 2018: Spatial patterns and regional integrals

355 The mean sea-air CO_2 fluxes of the pCO_2 products and GOBMs have very similar spatial patterns
356 when averaged over the 1985 to 2018 period (Figure 1c,d). The pCO_2 products show a weak CO_2
357 outgassing over large areas of the tropical regions of the South and North Atlantic, which is more
358 intense in the western equatorial Atlantic. In comparison, the GOBMs exhibit weaker CO_2 fluxes
359 in the equatorial region but more intense CO_2 fluxes in the Benguela and Mauritanian upwelling
360 areas. In these upwelling regions, the ocean circulation delivers nutrients and DIC to the surface
361 layer where they are consumed by photosynthesizing organisms. In many of these regions, the
362 supply of DIC from below exceeds the amount of DIC being drawn down by the net balance
363 between photosynthesis and remineralization/respiration, i.e., net community production, such that
364 an excess of DIC and nutrients remain at the surface, indicative of an inefficient biological pump
365 (Sarmiento and Gruber, 2006). As a result, these regions act as a source of CO_2 to the atmosphere.
366 Downstream of many of these regions, the remaining nutrients and the DIC get drawn down
367 completely. This resulting large increase in the biological pump efficiency makes these regions
368 strong uptake regions. The NA SPSS and NA STSS biomes, and the southern parts of biome SA
369 STPS are characterized by strong CO_2 uptake with some differences between the spatial patterns
370 modeled in the GOBMs and those derived from observations. In these regions both the cooling of
371 the warm poleward moving waters and an efficient and strong biological pump promote CO_2
372 uptake from the atmosphere (Watson et al. 1995, Thomas et al. 2008, Takahashi et al. 2009).

373 pCO_2 products and GOBMs agree remarkably well with respect to their zonally integrated
374 CO_2 fluxes south of 40°N (Figure 1b), while this breaks apart north of 52°N . There, GOBMs show
375 a more intense ocean uptake of CO_2 , coinciding with the deep convection regions in the subpolar
376 gyre (NA SPSS biome). In this region, models underestimate the transport and mixing of high
377 subsurface DIC water to the surface during winter, underestimating the winter-time outgassing
378 from the ocean (McKinley et al 2018). The results obtained with the ROBM are very similar to
379 that of the GOBMs between 35°S and 52°N , while it seems to overestimate uptake north of 52°N

380 even more than the GOBMs. The inverse model OCIMv2021 follows the large-scale pattern of the
381 other products, but shows more meridional variations and, similar to the ROBM, it also simulates
382 a much stronger uptake than seen in models and observations north of 52°N (Figure 1b).

383 As shown in Figure S1, the SOCAT gridded data of pCO₂ covers the NA SPSS biome with the
384 highest number of observations among the Atlantic biomes, resulting in an average of 10.2% of
385 the maximum possible coverage since 2003 and making it one of the regions where the pCO₂
386 products are expected to provide comparative robust results. The UOEX data product, that adjusts
387 the pCO₂ for near-surface temperature and salinity gradients, shows higher CO₂ uptake than the
388 ensemble mean of the other pCO₂ products between 35°S and 50°N due to the expected effect of
389 lower skin temperature on solubility. However, this effect is not observed in the subpolar gyre (lat
390 >52°N), being sometimes even opposite to expectations.



391 Integrated over the whole Atlantic Ocean, the average sea-air CO₂ flux (FCO₂) for the
 392 period 1985 to 2018 obtained from the GOBMs (-0.47 ± 0.15 PgC yr⁻¹) is higher than that obtained
 393 from the pCO₂ products (-0.37 ± 0.06 PgC yr⁻¹; Figure 2), although the difference is within the FCO₂
 394 variability across the 11 GOBMs. OCIMv2021 estimates a larger uptake (-0.58 ± 0.08 PgC yr⁻¹)
 395 than the GOBMs. The ROBM simulates an uptake of -0.61 ± 0.14 PgC yr⁻¹, about 30% and 65%
 396 stronger than the mean of the GOBMs and pCO₂ products, respectively. Relative to the mean of
 397 the pCO₂ products, the surface skin effects as represented in UOEX increases the CO₂ uptake by
 398 about 23%.

399

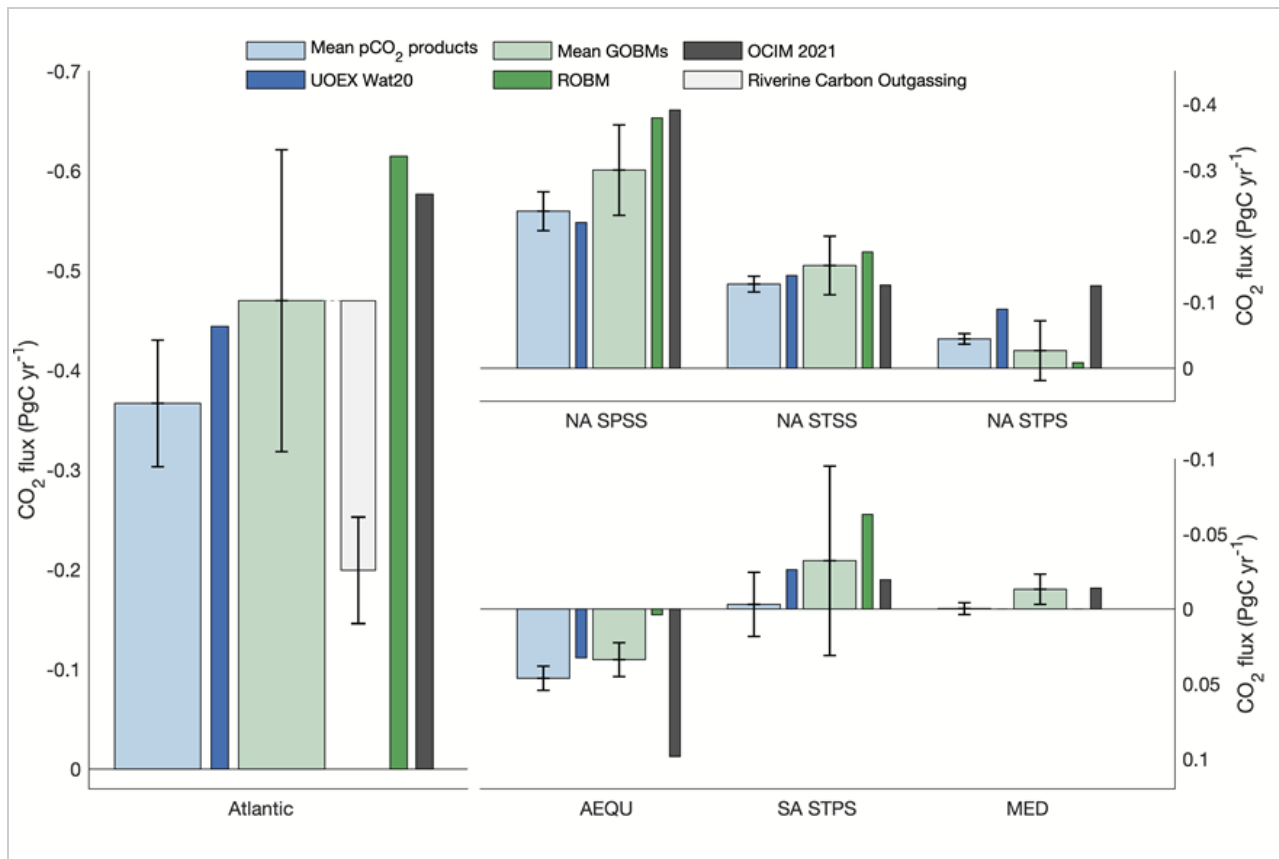


Figure 2. a) Spatially integrated sea-air CO₂ fluxes from 1985 to 2018 for the Atlantic and each Atlantic biome as estimated by nine pCO₂ products, ten GOBMS, the UOEX pCO₂-data product, the ROBM and OCIMv2021. The white bar indicates an estimate for the outgassing of riverine carbon integrated over the whole Atlantic region, which is a flux component captured by the pCO₂ products but not by the GOBMs or the ROBM. Whiskers stand for standard deviation around the mean of estimates. Negative values indicate uptake of CO₂ from the atmosphere. Note that the y-axes are reversed, so that uptake is above the zero-line and outgassing is below it.

400 The NA SPSS biome, which covers only 15% of the Atlantic Ocean surface area, has the
 401 largest CO₂ uptake and also the largest differences between models and observational products
 402 (Figures 1 and 2, Table 1). Here, the mean FCO₂ of the GOBMs, the ROBM and OCIMv2021

403 indicate 26, 59 and 64% greater carbon uptake, respectively, than the pCO₂ products. The spread
404 between GOBMs is three times larger than it is for the pCO₂ products (**Table S4**). The surface skin
405 effect as represented in UOEX leads to a slightly lower uptake flux (~7%) in relation to the mean
406 of pCO₂ products.

407 In the NA STSS biome, the agreement between the different pCO₂ products is remarkable,
408 with a standard deviation that is less than 10% of the mean (-0.13 ± 0.01 PgC yr⁻¹). Here, the UOEX
409 product has 10% larger CO₂ uptake. With an average FCO₂ of -0.15 ± 0.04 PgC yr⁻¹, the GOBMs
410 vary substantially more among each other, i.e., $\pm 30\%$. In fact, one GOBM has a ~50% weaker
411 uptake than the GOBMs mean, while the GOBMs with the most intense fluxes are only 20% above
412 the GOBMs mean. OCIMv2021 simulates FCO₂ values of similar magnitude to the pCO₂ products
413 (Table S4).

414 For the NA STPS biome, pCO₂ products estimate a mean CO₂ uptake of -0.044 ± 0.008 PgC
415 yr⁻¹ with a very high homogeneity in spite of the large area of this biome. In comparison to the
416 pCO₂ products, the uptake simulated by the GOBMs is smaller, (-0.020 ± 0.040 Pg/yr), and with
417 larger intermodel variations. Only three GOBMs estimated a CO₂ outgassing in this biome. In
418 contrast, OCIMv2021 reported a quite high uptake of CO₂, almost three times larger than that of
419 the pCO₂ products. The ROBM simulates a near-zero net flux in this biome. In the UOEX product,
420 the uptake is twice as large as the mean of the other pCO₂ products.

421 All models and pCO₂ products agree that the AEQU biome is a net source of CO₂ to the
422 atmosphere, consistent with the known impact of the equatorial upwelling that brings water with
423 high DIC content to the ocean surface. The mean flux of the pCO₂ products is 0.046 ± 0.009 PgC
424 yr⁻¹. In the UOEX product this outgassing is 25% lower. The mean flux in the GOBMs is
425 0.035 ± 0.011 PgC yr⁻¹, and has relatively small inter-model variations. The ROBM simulates a
426 very low outgassing. The OCIMv2021 shows strong FCO₂, with more than twice the outgassing
427 of the mean GOBMs.

428 The SA STPS biome covers a large area, extending from the southern border of the
429 equatorial region in the north towards the subtropical front of the Southern Ocean in the south.
430 According to the mean of the pCO₂ products, the integrated flux over this region is neither a sink
431 nor source of CO₂ to the atmosphere (-0.003 ± 0.023 PgC yr⁻¹). But, the spread across the pCO₂
432 products is relatively large in this region, second only to the spread in the NA SPSS, in part because
433 of the large area of the SA STPS biome. On average the GOBMs indicate that this region is a CO₂
434 sink with an estimated integrated flux of -0.029 ± 0.076 PgC yr⁻¹. However, an integrated outgassing
435 is simulated by 1/3 of the GOBMs. The FCO₂ in the ROBM is nearly twice as large as the mean
436 of the GOBMs, while the OCIMv2021 suggested that the region behaves as a weaker CO₂ sink.

437 In the Mediterranean Sea, only five of the nine pCO₂ products have a regional coverage
438 better than 95%. These four pCO₂ products agree that the biome does not present significant sea-
439 air CO₂ fluxes (Figure 2 and Table S4). Most of the GOBMs have a coverage better than 95% and
440 they broadly agree that the Mediterranean Sea represents a very weak CO₂ sink (-0.015 ± 0.010 PgC
441 yr⁻¹). The flux in the OCIMv2021 is very similar. The ROBM has insufficient regional coverage

442 for an assessment in this biome.

443 In summary, for the Atlantic, the GOBMs predict a $28\pm 14\%$ larger CO_2 uptake than pCO_2
 444 products (Table 1). The regional and data-assimilation models simulate a stronger Atlantic CO_2
 445 sink than pCO_2 products by 67 and 57%, respectively (Table S4). The same is the case for the
 446 UOEX product, where the CO_2 uptake is 25% larger than that of the mean pCO_2 products, as a
 447 consequence of its adjustment for near surface temperature gradients.

448

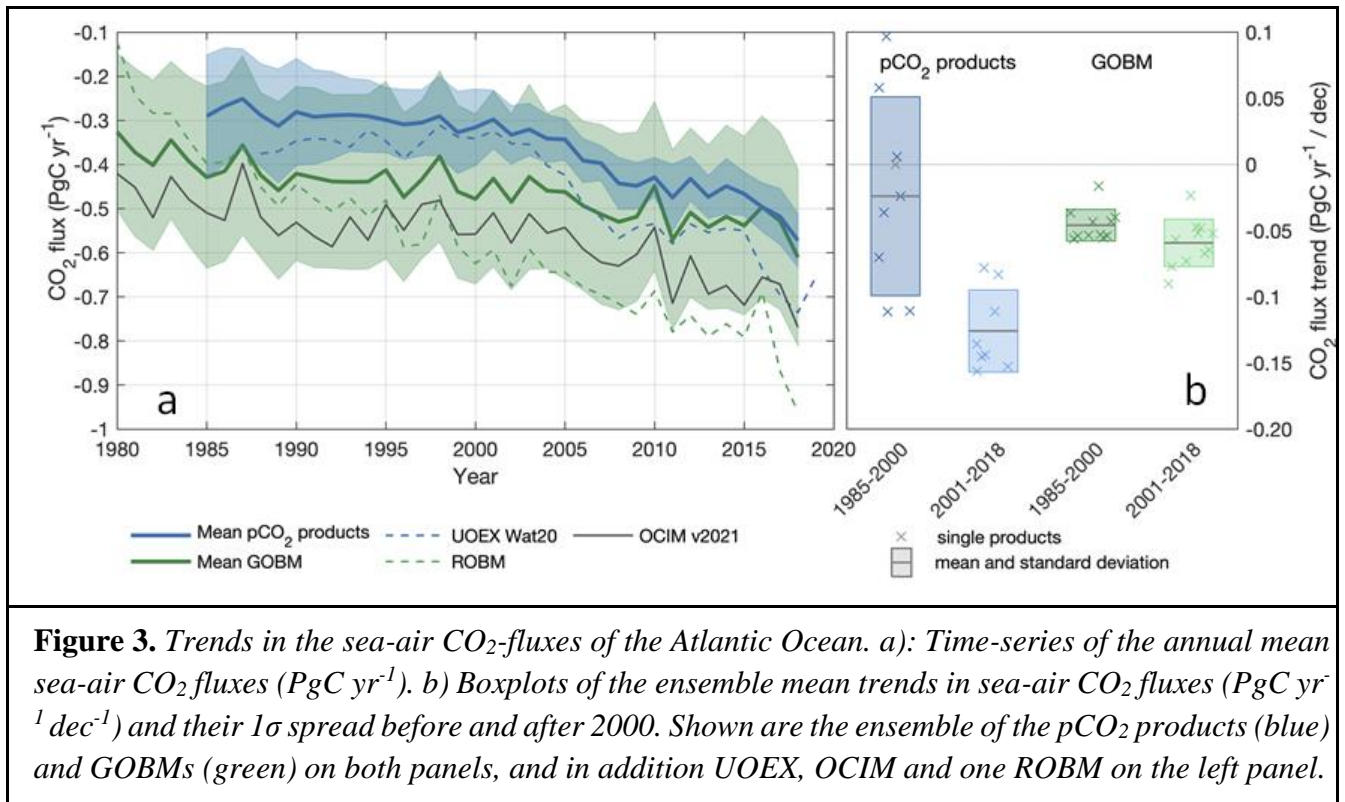
449 3.1.2 FCO_2 trends

450 The temporal evolution of the annual mean sea air fluxes in the pCO_2 products shows a
 451 change of rate around the year 2000 (Figure 3). In agreement with the recommended core analysis
 452 in RECCAP2, we thus analyzed the changes in FCO_2 during two periods; between 1985 and 2000,
 453 and between 2001 and 2018. Over these two periods, the atmospheric CO_2 concentration increased
 454 on average by 1.5 and 2.1 ppm yr^{-1} , respectively, representing an acceleration in the atmospheric
 455 growth rate of 43% from the first to the second period. Integrated over the Atlantic as a whole, the
 456 pCO_2 products indicate a 5-fold increase in the growth rate of the ocean carbon sink from
 457 $-0.024\pm 0.075 \text{ PgC yr}^{-1} \text{ dec}^{-1}$ between 1985 and 2000 to $-0.126\pm 0.031 \text{ PgC yr}^{-1} \text{ dec}^{-1}$ between 2001
 458 and 2018 (Figure 3). In contrast, GOBMs simulate only a 33% increase in the growth rate between
 459 the two periods, i.e., from $-0.045\pm 0.012 \text{ PgC yr}^{-1} \text{ dec}^{-1}$ between 1985 and 2000 to -0.060 ± 0.017
 460 $\text{PgC yr}^{-1} \text{ dec}^{-1}$ between 2001 and 2018 (Figure 3). This is only slightly below the observed
 461 acceleration in the atmospheric CO_2 growth rate. The two products differ also strongly with regard
 462 to their spreads (Figure 3b): While the pCO_2 products exhibit a relatively low spread for the 1985-
 463 2018 mean flux, they differ considerably with regard to their FCO_2 trends. Conversely, GOBMs
 464 show large spread in the 1985-2018 mean flux, but have a low spread in their FCO_2 trends in both
 465 periods, reflecting that the trends in the GOBMs are more strongly governed by the rate of change
 466 in atmospheric CO_2 .

467 The CO_2 uptake trend increases in OCIMv2021 from -0.045 ± 0.016 during the first period
 468 to $-0.111\pm 0.018 \text{ PgC yr}^{-1} \text{ dec}^{-1}$ for the second period. Its estimate is thus similar to that of the
 469 GOBMs in the first period but almost twice as large in the second. The ROBM simulates a much
 470 stronger growth than the GOBMs in both periods (-0.19 ± 0.02 and $-0.14\pm 0.02 \text{ PgC yr}^{-1} \text{ dec}^{-1}$, but
 471 no significant change in trend). On the other hand, the UOEX pCO_2 product reveals an even greater
 472 contrast between the growth rates before 2000 ($0.048\pm 0.014 \text{ PgC yr}^{-1} \text{ dec}^{-1}$) and after 2000 ($-$
 473 $0.188\pm 0.012 \text{ PgC yr}^{-1} \text{ dec}^{-1}$) than the ensemble mean of the pCO_2 products. The trends obtained by
 474 the UOEX product showed a weakening of CO_2 uptake in the Atlantic Ocean before 2000, and an
 475 increase of about 0.35 PgC yr^{-1} in the second period, which is higher than in any of the other eight
 476 pCO_2 products (range: 0.14 to 0.28 PgC yr^{-1}). Three of the other pCO_2 products also suggest a
 477 weakening of the CO_2 uptake in the Atlantic before 2000, while four other products suggest
 478 increasing trends in CO_2 uptake by the Atlantic. Possibly the sharp contrast in observational
 479 coverage before and after the year 2000 (Figure S1; Bakker et al 2022), as well as the availability
 480 of observed predictor data affected in a noticeable way some of the products. In fact, the pCO_2

481 products agree increasingly better over the 1985-2000 period, showing that unlike the GOBMs,
 482 the trends in the first period are strongly conditioned by the FCO₂ estimates in the early years
 483 (Figure S2) when, in addition to having few pCO₂ observations, some products have used
 484 climatologies of some predictors such as chlorophyll and mixed layer depth because of lack of
 485 observations.

486



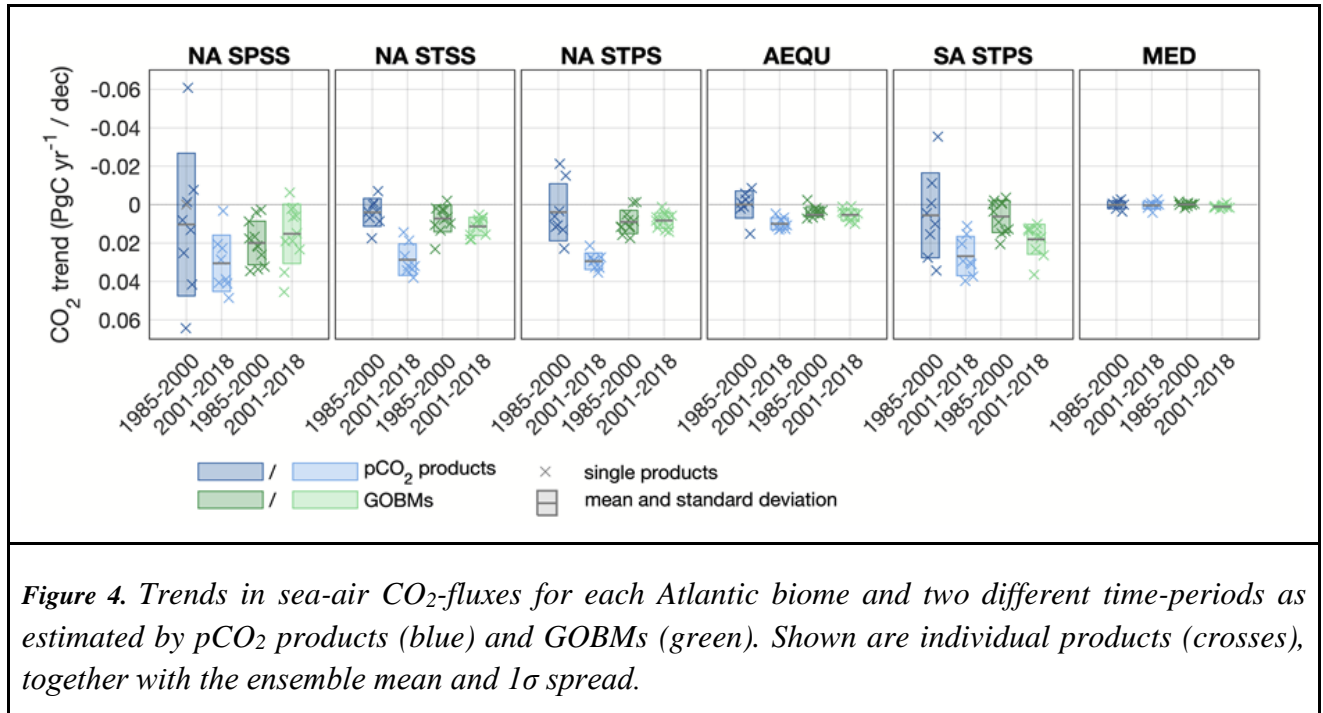
487

488 Temporal trends in the individual biomes of the Atlantic are variable and highly dependent
 489 on the products used to estimate them (see Figure 4 and Table S5). Between 2001 and 2018, the
 490 pCO₂ products show that the CO₂ uptake rate grows with values close to -0.03 PgC yr⁻¹ dec⁻¹ in
 491 the NA SSPS, NA STSS, NA STSS and SA STPS biomes (which present very different areas) and
 492 -0.01 PgC yr⁻¹ dec⁻¹ in the AEQU biome. During this period after 2000, all pCO₂ products agree
 493 on the sign of the trend in all biomes, with the exception of the MED biome where the trend was
 494 consistently close to zero. However, for the period 1985-2000, trends in CO₂ uptake estimated by
 495 the pCO₂ products are more variable across the different products and biomes, with non-significant
 496 trends in FCO₂ in NA STPS (-0.004±0.015 PgC yr⁻¹ dec⁻¹), AEQU (0.000±0.001 PgC yr⁻¹ dec⁻¹),
 497 and SA STPS (-0.006±0.022 PgC yr⁻¹ dec⁻¹) and remarking a notable contrast between the two
 498 periods.

499 The biome-level trends are more consistent across the GOBMs than across the pCO₂
 500 products, and also more similar in the two periods. In three biomes, NA STSS, AEQU and SA

501 STSS, the GOBMs simulate on average an increase in fluxes to the ocean between the first and the
 502 second period. The disagreement among the GOBMs and between GOBMs and pCO₂ products is
 503 largest in the NA SPSS biome. The ROBM shows rates of increase of CO₂ uptake higher than -
 504 0.03 PgC yr⁻¹ dec⁻¹ in practically all biomes and in both periods except in NA STPS in the second
 505 one, and AEQU biomes in both (see Table S5). OCIMv2021 shows similar rates of increase to
 506 those observed in pCO₂ products for the second period, except in MED, where it estimates an
 507 increase in CO₂ uptake rate in line with the ROBM (Table S5).

508



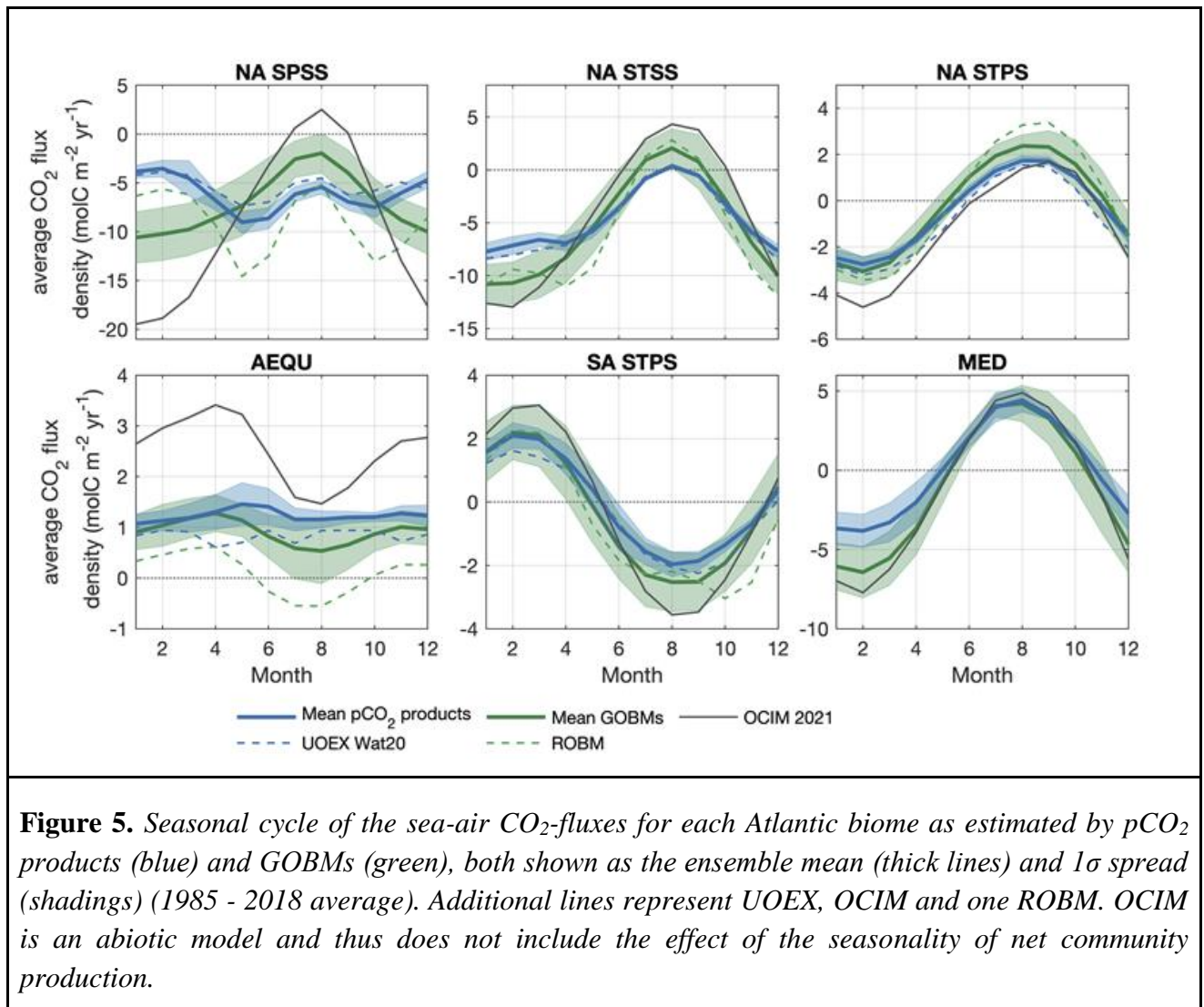
509

510 3.1.3 Seasonal cycle

511 The Atlantic Ocean sea-air CO₂ flux varies seasonally in a pronounced manner in all
 512 biomes, except for the equatorial (Figure 5). The Mediterranean Sea and the subtropical biomes
 513 (in their respective hemispheres) are CO₂ sinks in winter and sources in summer. Here, the impact
 514 of biological DIC drawdown on pCO₂ is relatively weak and seasonal warming and cooling
 515 dominates the seasonal cycle such that it peaks and reaches supersaturation in summer while
 516 minimum and undersaturated values occur in winter (Figure S3, S4 and Rodgers et al., in review).
 517 The seasonal amplitude in the flux in these regions is slightly larger in the GOBMs than in the
 518 pCO₂ products. This has been attributed to a likely underestimation of seasonal mixed layer depth
 519 changes and seasonal drawdown of DIC by net primary production, such that the thermal
 520 component on the seasonal pCO₂ and sea-air CO₂ flux cycle is too strong in these models (Rodgers
 521 et al., in review). The OCIMv2021 is an abiotic model and shows the largest seasonal pCO₂ (Figure
 522 S3) and flux variations because of the complete absence of biological processes. The difference in

523 the seasonal cycle as modeled by the OCIMv2021 and the other GOBMs can be taken as a rough
 524 estimate of the importance of biology.

525



526

527 In the NA SPSS biome, the GOBMs' seasonal CO₂ flux cycle is similar to that in the
 528 subtropical biomes (and of the abiotic OCIM model), while that of the pCO₂ products is broadly
 529 reversed, apart from the summertime intermediate minimum in CO₂ uptake (Figure 5). The pCO₂
 530 products have the highest pCO₂ values in winter, as a consequence of deep mixing (Figure S3).
 531 The spring bloom then causes a sharp decrease from March to June, after which the pCO₂ steadily
 532 increases back to its winter maximum. The existence of these patterns is well known from the
 533 many direct observations in this region (Takahashi et al., 1993; Olsen et al., 2008; Fröb et al.,
 534 2019, Becker et al., 2018). The opposite seasonal pCO₂ cycle in the GOBMs, is likely due to the
 535 fact that their seasonal variations in mixed layer depths are too small (Rodgers et al., in review) -

536 too few nutrients are brought up from the deep in winter- such that the summer biological
537 drawdown of DIC is likely underestimated in the GOBMs (Rodgers et al., in review; also shown
538 for Earth System Models in Goris et al., 2018). Since the opposing seasonal cycle of the GOBMs
539 leads to a pCO₂ underestimation at the time of the strongest wind speeds, the GOBMs ensemble
540 overestimates the annual net NA SPSS CO₂ uptake (Figures 1 and 2), i.e., the GOBMs tend to
541 simulate a too strong uptake. Again, the OCIMv2021, as an abiotic model, is an extreme example
542 of these model-effects. The ROBM appears more consistent with the pCO₂ products in this regard,
543 but it overall appears to overestimate the NA SPSS CO₂ uptake as the modeled pCO₂ values are
544 too low (Figure S3). The summertime intermediate minimum in CO₂ uptake in the pCO₂ products
545 is a consequence of the minimum in wind speeds in that season. More quantitative analyses of the
546 seasonal cycle including their drivers and differences between GOBMs and pCO₂ products are
547 presented by Rodgers et al. (in review).

548

549 3.1.4 Interannual Variability of the sea-air CO₂ fluxes

550 We further analyzed the interannual variability (IAV) of sea-air CO₂ fluxes, determined as
551 the annual anomaly of the detrended sea-air CO₂ fluxes with respect to their mean values. Here,
552 the removed linear trends and means are considered over the period 1985-2018 for pCO₂ products
553 and GOBMs. When referencing the amplitude of IAV, we here refer to the standard deviation of
554 the so-derived detrended air-sea CO₂ flux anomalies. We find that, over the whole Atlantic basin,
555 the IAV time-series of the sea-air CO₂ fluxes of GOBMs and pCO₂ products correlate relatively
556 well (Figure 6d). Furthermore, both pCO₂ products and GOBMs show a high IAV amplitude in
557 the northern parts and low IAV amplitude in the equatorial region (Figure 6a,b). This general
558 spatial pattern of the IAV amplitude of net sea-air CO₂ fluxes has also been found in other studies
559 (Brady et al., 2019; Park et al., 2010). Yet, the GOBMs show a larger IAV amplitude than the
560 pCO₂ products in the interior subpolar gyre as well as in the eastern boundary upwelling regions
561 (Figure 6a,b), while showing a smaller IAV amplitude for the NA SPSS biome as a whole (Figure
562 6e).

563 The pCO₂ products and GOBMs agree on the phasing of the IAV in net sea-air CO₂ fluxes,
564 apart from in the subpolar region where correlations are small and negative (Figure 6c, e; Figure
565 S5). We note that there is also little agreement in the IAV of this biome between pCO₂ products
566 (Figure S7), while the GOBMs agree relatively well (Figure S6). GOBMs and pCO₂ products agree
567 that the total sea-air CO₂ fluxes of the biomes NA STSS, NA STPS and SA STPS are characterized
568 by a moderate IAV amplitude (Figure S6), and that biomes AEQU and MED have only a weak
569 IAV amplitude (see Figure S5). For these five biomes, GOBMs and pCO₂ products correlate
570 reasonably well with respect to the temporal variability of the IAV with correlations coefficients
571 ranging from $r=0.57$ to $r=0.73$ (see also Figure S5).

572

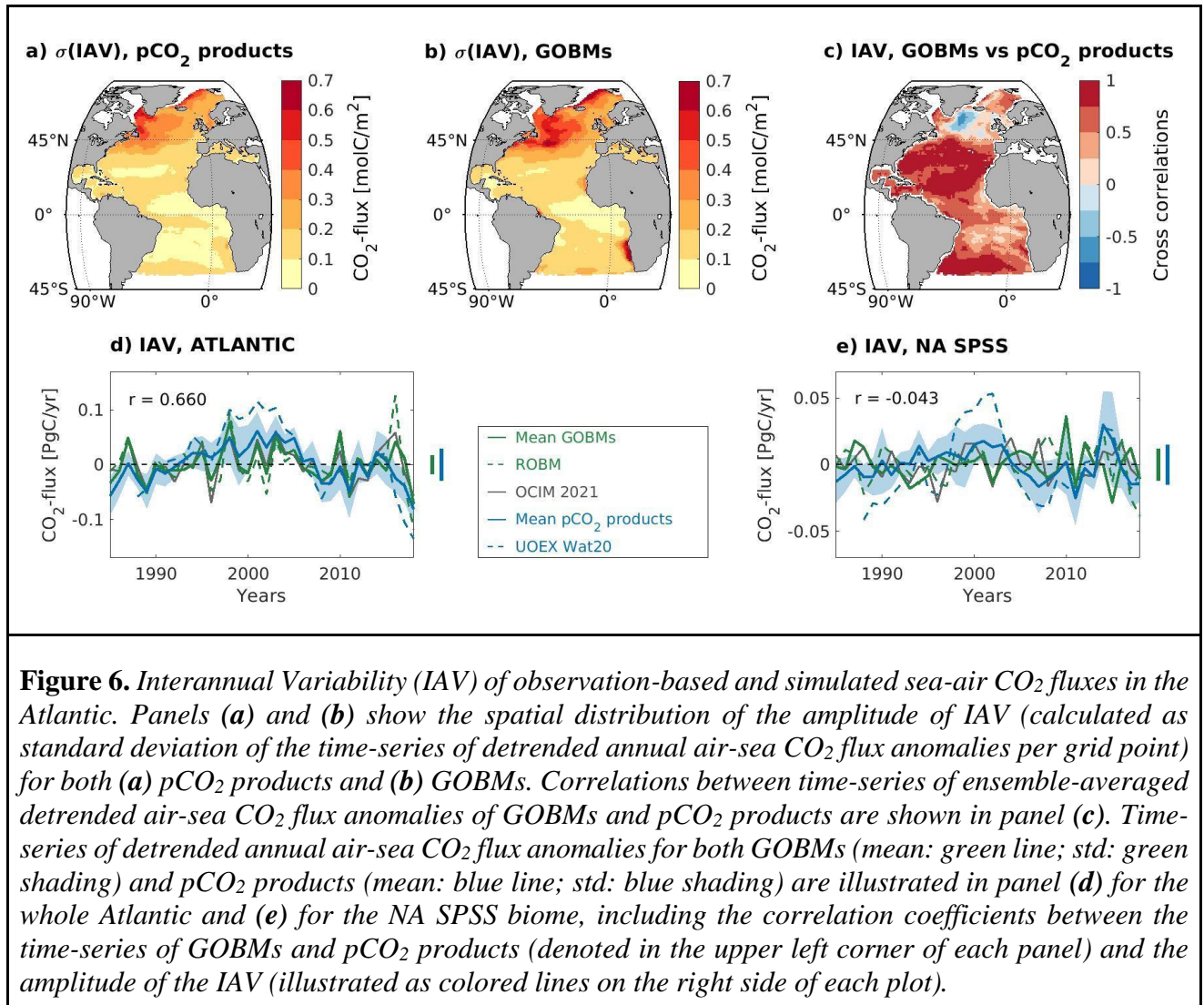


Figure 6. Interannual Variability (IAV) of observation-based and simulated sea-air CO₂ fluxes in the Atlantic. Panels (a) and (b) show the spatial distribution of the amplitude of IAV (calculated as standard deviation of the time-series of detrended annual air-sea CO₂ flux anomalies per grid point) for both (a) pCO₂ products and (b) GOBMs. Correlations between time-series of ensemble-averaged detrended air-sea CO₂ flux anomalies of GOBMs and pCO₂ products are shown in panel (c). Time-series of detrended annual air-sea CO₂ flux anomalies for both GOBMs (mean: green line; std: green shading) and pCO₂ products (mean: blue line; std: blue shading) are illustrated in panel (d) for the whole Atlantic and (e) for the NA SPSS biome, including the correlation coefficients between the time-series of GOBMs and pCO₂ products (denoted in the upper left corner of each panel) and the amplitude of the IAV (illustrated as colored lines on the right side of each plot).

573

574 For the GOBMs ensemble, the IAV of net sea-air CO₂ fluxes is strongly positively
 575 correlated to the IAV in SST (more FCO₂ in anomalously warm years) over large parts of the
 576 Atlantic basin; most notably for both permanently stratified biomes (SA STPS and NA STPS) and
 577 the northwestern subpolar gyre (Figure S8b). Along the Gulf Stream and the North Atlantic
 578 Current as well as regions of equatorial upwelling, the IAV in net sea-air CO₂ fluxes of the GOBMs
 579 ensemble is weakly negatively correlated to the IAV in SST (more FCO₂ in anomalously cold
 580 years). Due to the known dynamics of net sea-air CO₂ fluxes, these negative correlations imply
 581 that SST-variations are not the main driver of the IAV in net sea-air CO₂ fluxes but that the
 582 anomalous cold years are likely accompanied by stronger mixing and hence more DIC upwelling.
 583 As the thermodynamic boundary conditions used to force the GOBMs result in SSTs that have
 584 relatively strong fidelity to observations when averaged over biome scales, it is plausible that the
 585 relatively small model spread around the IAV in the Atlantic is related to the fact that most of the
 586 simulated IAV is driven by SST-variations (areas with positive correlations in Figure S8b) and

587 that variations in DIC play a less important role. The strong relationship to SST is also the plausible
 588 cause for high correlations between IAV in net sea-air CO₂ fluxes of pCO₂ products and GOBMs
 589 in SA STPS and NA STPS. Indeed, when correlating the IAV in net sea-air CO₂ fluxes of pCO₂
 590 products to the IAV in SST (Figure S8a), we find strong correlations in SA STPS and NA STPS
 591 biomes. However, in the NA SPSS, the pCO₂ products appear to be more negatively correlated to
 592 the IAV in SST (likely driven by DIC-variations), in contrast to the GOBMs. This difference in
 593 mechanisms over the subpolar gyre is one possible explanation for the disagreement in the IAV in
 594 net sea-air CO₂ fluxes between pCO₂ products and GOBMs in the NA SPSS biome.

595 In the North Atlantic, one of the most prominent climate variability modes at interannual
 596 time scales is the NAO. In a study about the influences of NAO on the IAV of North Atlantic CO₂
 597 fluxes, Jing et al. (2019) noted that, in summer, SST is important for the IAV in pCO₂ in the
 598 subtropical North Atlantic, while biogeochemical variables probably control the pCO₂ IAV in the
 599 subpolar North Atlantic. When relating the IAV of the GOBMs to NAO, we find significant but
 600 weak correlations for the NA SPSS and the AEQU biomes ($r=-0.43$, $p=0.01$ and $r=-0.48$, $p=0.004$),
 601 whereas all other biomes show no significant correlation to the NAO index. Yet, the pCO₂ products
 602 show a similar correlation between NAO and IAV for the AEQU biome ($r=-0.41$, $p=0.02$), but no
 603 significant correlation in the NA SPSS biome (neither for the average nor for single products). The
 604 absent correlation in the NA SPSS could be due to the opposing imprints of NAO on pCO₂ in the
 605 western and eastern domains of NA SPSS. In their modeling study, Tjiputra et al. (2012)
 606 demonstrated that during positive NAO, SST cooling induces negative pCO₂ anomaly in the
 607 western subpolar gyre, whereas in the eastern part (in the proximity of the Irminger Sea)
 608 anomalously deep winter mixing upwells DIC-rich watermass and induces positive pCO₂ anomaly
 609 (e.g., Fröb et al., 2019). The opposite mechanism is suggested during negative NAO.

610 We note that despite relatively high correlations between IAV of GOBMs and pCO₂
 611 products in all biomes apart from the NA SPSS (Figure 6c), the amplitude of the IAV of the
 612 GOBMs is smaller than that of pCO₂ products in all biomes except the NA STSS (Figure S5). The
 613 amplitude of the IAV of the total sea-air CO₂ fluxes in the Atlantic basin is 0.029 ± 0.01 PgC yr⁻¹
 614 (pCO₂ products) and 0.018 ± 0.005 PgC yr⁻¹ (GOBMs). These results are significantly different
 615 but of similar magnitude as the linear trends of the sea-air CO₂ fluxes of the Atlantic basin (Figure
 616 3). For a better estimate of the sea-air CO₂ fluxes in the Atlantic basin, it is hence important to
 617 have an accurate estimate of both temporal variability and amplitude of the IAV, which is currently
 618 not adequately represented. Moreover, the temporal disagreement of IAV of pCO₂ products in the
 619 NA SPSS makes it clear that a closer examination of the gap filling methods and their dynamic
 620 realism is urgently needed here (Hauck et al., 2023, Gloege et al., 2021).

621 3.2 Ocean interior C_{ant} accumulation from 1994-2007

622 The rate of anthropogenic carbon accumulation (ΔC_{ant}) was evaluated for the period 1994-2007
 623 for comparison between GOBMs, the data-assimilation model OCIMv2021 and two ΔC_{ant}
 624 reconstruction products. Nine of the ten GOBMs simulated an increasing ΔC_{ant} inventory for the
 625 time-frame considered (see Figure S9), and are broadly consistent among themselves and with

626 observations (Table S6). Seven models show high C_{ant} accumulations in the NA SPSS biome and
 627 in the NA STSS, consistent with the ΔC_{ant} reconstruction products, while the other two
 628 (PlankTOM12 and CESM-ETHZ) show high C_{ant} accumulations in the vicinity of 35°S, but very
 629 weak accumulation in the North Atlantic. The MPIOM-HAMOCC was excluded from the analysis
 630 of ΔC_{ant} (see Section 2.2).

631

Table 1. Sea-air surface CO₂ fluxes (1985-2018) and anthropogenic CO₂ accumulation rates (1994-2007) of all products used in this study. Respective standard deviations are in light gray (see Methods). For ΔC_{ant} the MED biome is not included in the total Atlantic estimate to facilitate direct comparison with Gruber et al. (2019). The surface area of each region (in m²) is given below the region's name.

FCO₂ [1985 – 2018] (PgC yr ⁻¹)	ATLANTIC (68.7 · 10 ¹²)	NA SPSS (9.37 · 10 ¹²)	NA STSS (6.14 · 10 ¹²)	NA STPS (22.7 · 10 ¹²)	Atl EQU (8.69 · 10 ¹²)	SA STPS (19.6 · 10 ¹²)	Med (2.26 · 10 ¹²)
Ensemble mean	-0.37 ±0.06	-0.24 ±0.03	-0.127 ±0.012	-0.044 ±0.008	0.046 ±0.008	-0.003 ±0.021	0.000 ±0.005
GOBMs							
Ensemble mean	-0.47 ±0.15	-0.30 ±0.07	-0.149 ±0.041	-0.020 ±0.041	0.035 ±0.011	-0.029 ±0.065	-0.015 ±0.009
ROBM							
ROMS-ETHZ	-0.61 ±0.15	-0.38 ±0.05	-0.176 ±0.022	-0.008 ±0.026	0.004 ±0.016	-0.063 ±0.040	-
Assim. model							
OCIMv2021	-0.58 ±0.08	-0.40 ±0.03	-0.126 ±0.012	-0.125 ±0.024	0.098 ±0.005	-0.020 ±0.022	-0.014 ±0.003
ΔC_{ant} (PgC yr⁻¹)							
GOBMs							
Ensemble mean	0.52±0.11	0.087 ±0.033	0.080 ±0.031	0.175 ±0.045	0.037 ±0.006	0.127 ±0.018	0.018 ±0.007
Assim. model							
OCIMv2021	0.68 ±0.01	0.127 ±0.001	0.107 ±0.001	0.236 ±0.002	0.054 ±0.001	0.156 ±0.001	0.019 ±0.000
C_{ant} reconstruction							
Gruber et al., 2019	0.72 ±0.08	0.087 ±0.007	0.098 ±0.005	0.254 ±0.017	0.058 ±0.018	0.216 ±0.041	-
Khawwala et al.,	0.63 ±0.11	0.149 ±0.027	0.105 ±0.018	0.199 ±0.036	0.040 ±0.007	0.137 ±0.025	

632

633 The spatial distribution of the column-integrated ΔC_{ant} averaged across the remaining nine
 634 GOBMs is shown in Figure 7b. The ΔC_{ant} column inventory distribution obtained by the
 635 OCIMv2021 inverse-model (Figure 7c) shows a very similar pattern to the GOBMs multi-model
 636 mean but with higher values throughout the Atlantic, except in the region of the Brazil Current and
 637 in the vicinity of the Azores Islands. In addition, OCIMv2021 produces a similar pattern to that
 638 obtained from the DIC-based product from Gruber et al., (2019) (Figure 7a), but with stronger
 639 (weaker) ΔC_{ant} in the north (south). The comparison between the GOBMs ensemble mean and the
 640 Gruber et al., (2019) observation-based product (Figure 7d) reveals that the GOBMs simulate
 641 slightly higher ΔC_{ant} than the observational product in the subpolar North Atlantic. In contrast,
 642 over the tropical and South Atlantic, the ΔC_{ant} column inventory of the GOBMs ensemble is only
 643 about half as high as the reconstruction of Gruber et al. (2019), highlighting the main discrepancies
 644 between both products.

645 Integrated over the whole Atlantic Ocean, the ΔC_{ant} inventory simulated by the GOBMs
646 ensemble (Table 1) is about $28 \pm 20\%$ lower than the inventory estimate obtained with the
647 observation-based eMLR(C^*) method (Gruber et al. 2019), 17% lower than the age-tracer based
648 method (Khatiwala et al., 2009), and $28 \pm 15\%$ lower than the inverse model OCIMv2021. By
649 contrast, the OCIMv2021 ΔC_{ant} inventory is very similar to Gruber et al., (2019), while 8% higher
650 compared to Khatiwala et al. (2009).

651 Integrated over the individual biomes of the Atlantic, we found the best agreement between
652 the GOBMs ensemble and the estimate from Gruber et al. (2019) in the northern biomes. In the
653 NA SPSS and NA STSS biomes, C_{ant} accumulation rates are very similar between GOBMs, and
654 only two models show extraordinarily low values (50% lower than the GOBMs average; Table
655 S6). In contrast, OCIMv2021 simulates a ΔC_{ant} inventory that is about 40% higher than the
656 observation-based estimate and the GOBMs ensemble mean, and therefore closer to the values
657 obtained with the Green's Function (Khatiwala et al., 2009). Further south, discrepancies between
658 the GOBMs-based and the observation-based ΔC_{ant} inventories increase, bringing the GOBMs
659 inventories closer to the age-tracer based product, while OCIMv2021 resembles the eMLR(C^*)-
660 based estimates in two of the three remaining biomes. In the NA STPS biome, characterized by
661 the largest inter-GOBMs spread, the ΔC_{ant} inventory of the GOBMs is about 25% lower than the
662 observation-based product, while the OCIMv2021 inventory reveals a similar rate of change as the
663 observation-based product. Likewise, in the AEQU biome, the GOBMs ensemble mean ΔC_{ant}
664 inventory is approximately 30% lower than that from Gruber et al. (2019) and OCIMv2021. The
665 AEQU biome further reveals the lowest ΔC_{ant} inventories with a very narrow inter-GOBMs spread.
666 The largest ΔC_{ant} inventory difference between the GOBMs and the observation-based product
667 exists in the SA STPS biome, with a GOBMs C_{ant} storage rate nearly 50% lower than that of Gruber
668 et al. (2019). In addition, in the SA STPS biome, the OCIMv2021 ΔC_{ant} inventory is also 30%
669 lower than that of Gruber et al. (2019). No comparison is done for the MED biome because of the
670 lack of data in ΔC_{ant} reconstruction products.

671 Average ΔC_{ant} vertical profiles of each biome and for the whole Atlantic (Figure S10)
672 reveal that the maximum C_{ant} accumulation occurs near the surface, while the accumulation rates
673 decrease rapidly with depth. In general, GOBMs simulations and the estimates from Gruber et al.
674 (2019) agree with regard to this vertical distribution, both in the Atlantic and at biome-level.
675 However, in the NA STPS, AEQU and SA STPS biomes, the observation-based reconstruction
676 presents a second ΔC_{ant} maximum between 1400 and 3000 m depths that is associated with waters
677 with moderate values of C_{ant} transported by the DWBC circulating southward below the Antarctic
678 Intermediate Water ΔC_{ant} minimum (Rhein et al. 2015; Fajar et al. 2015; Rios et al. 2012; Rios et
679 al. 2003), generally not simulated by the GOBMs. Thus, the underestimation of C_{ant} accumulation
680 rate by GOBMs in the South Atlantic, compared to the observation-based reconstruction (Fig.
681 7a,7b), can be attributed to this bias in the interior accumulation rate below 1400 m, coinciding
682 with the depth wherein North Atlantic Deep Water (NADW) resides.

683

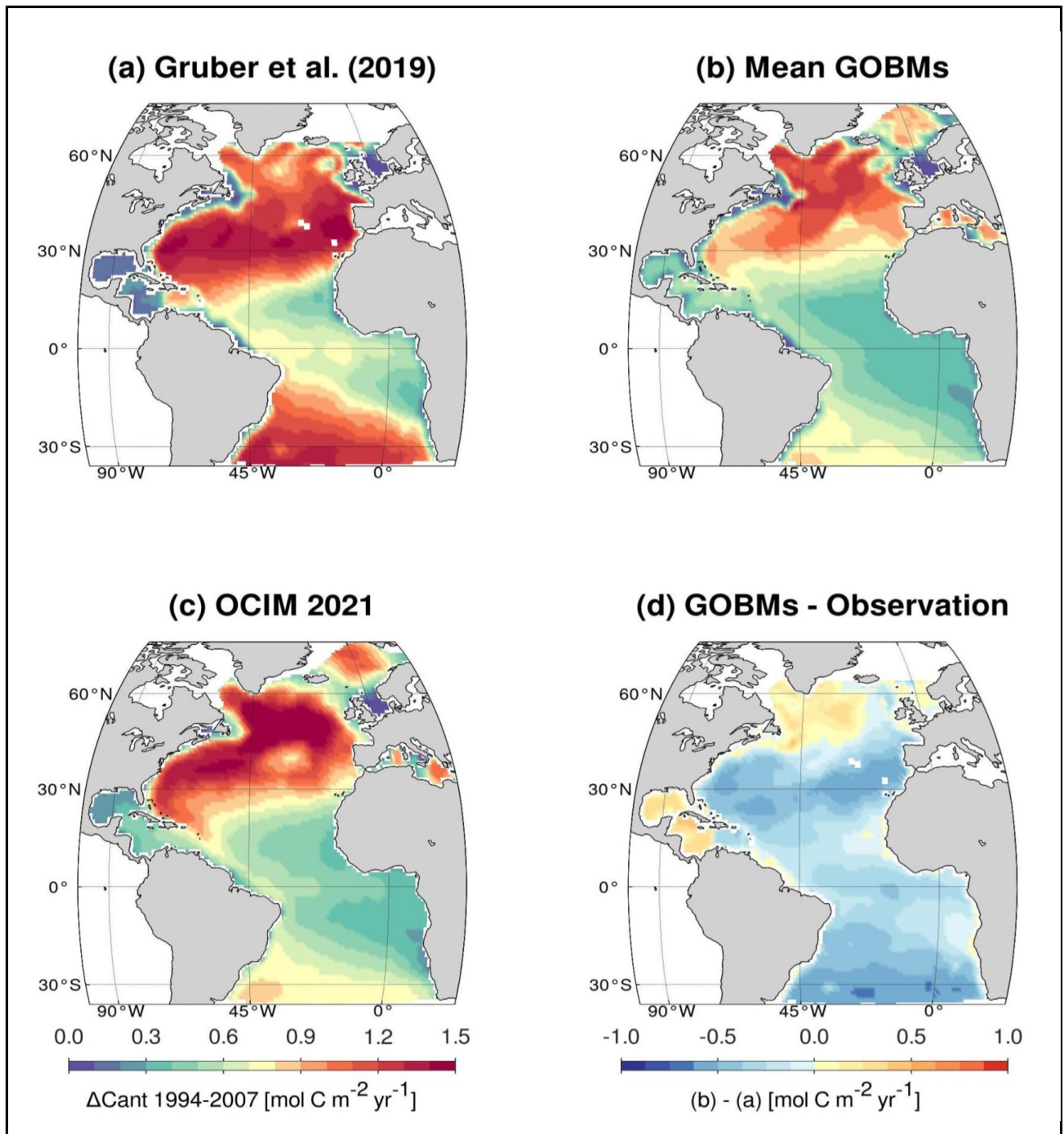


Figure 7. Column inventories of anthropogenic carbon storage changes (ΔC_{ant}), integrated from surface to 3000 m. Shown are C_{ant} changes from 1994 to 2007 for **a)** an observation-based reconstruction with the eMLR(C^*) method by Gruber et al. (2019); **b)** multi-model GOBMs ensemble mean **c)** OCIMv2021. Panel **d)** illustrates the difference between the estimates from GOBMs and Gruber et al. (2019).

685 3.3 Anthropogenic CO₂ uptake and lateral transport

686 In terms of recent storage changes in C_{ant} , GOBMs tend to simulate lower accumulation
 687 rates than observation-based estimates (Section 3.2), whereas we have previously described that
 688 the net CO₂ uptake is larger in GOBMs than pCO₂ products (Section 3.1.1). To assess this apparent
 689 inconsistency, the anthropogenic component of the CO₂ fluxes in GOBMs is assessed from the
 690 differences of Simulation A minus Simulation D in each GOBM, allowing us to determine the air-
 691 sea fluxes caused solely by increased CO₂ in the atmosphere. The anthropogenic FCO₂ averaged
 692 across 9 GOBMs (F_{ant}) in the Atlantic as a whole is shown in Figure 8 and for each of the biomes
 693 in Figure S11. Integrated over the whole Atlantic, the FCO_{2-ant} fluxes are lower in magnitude than
 694 the net flux FCO₂ because the natural flux component also contributes additional CO₂ uptake in
 695 the NA SPSS and NA STSS biomes. In the other biomes the natural contributions are lower or
 696 even represent positive fluxes (outgassing) (Figure S11). However, the net result for the Atlantic
 697 Ocean is a net uptake of natural CO₂ (approx $\sim 0.1 \text{ PgC yr}^{-1}$) being transported to the Southern
 698 Ocean. In terms of C_{ant} , the biome with the highest uptake is also the NA SPSS, although the
 699 latitudinal variability is by far not as marked as in the natural component of FCO₂.

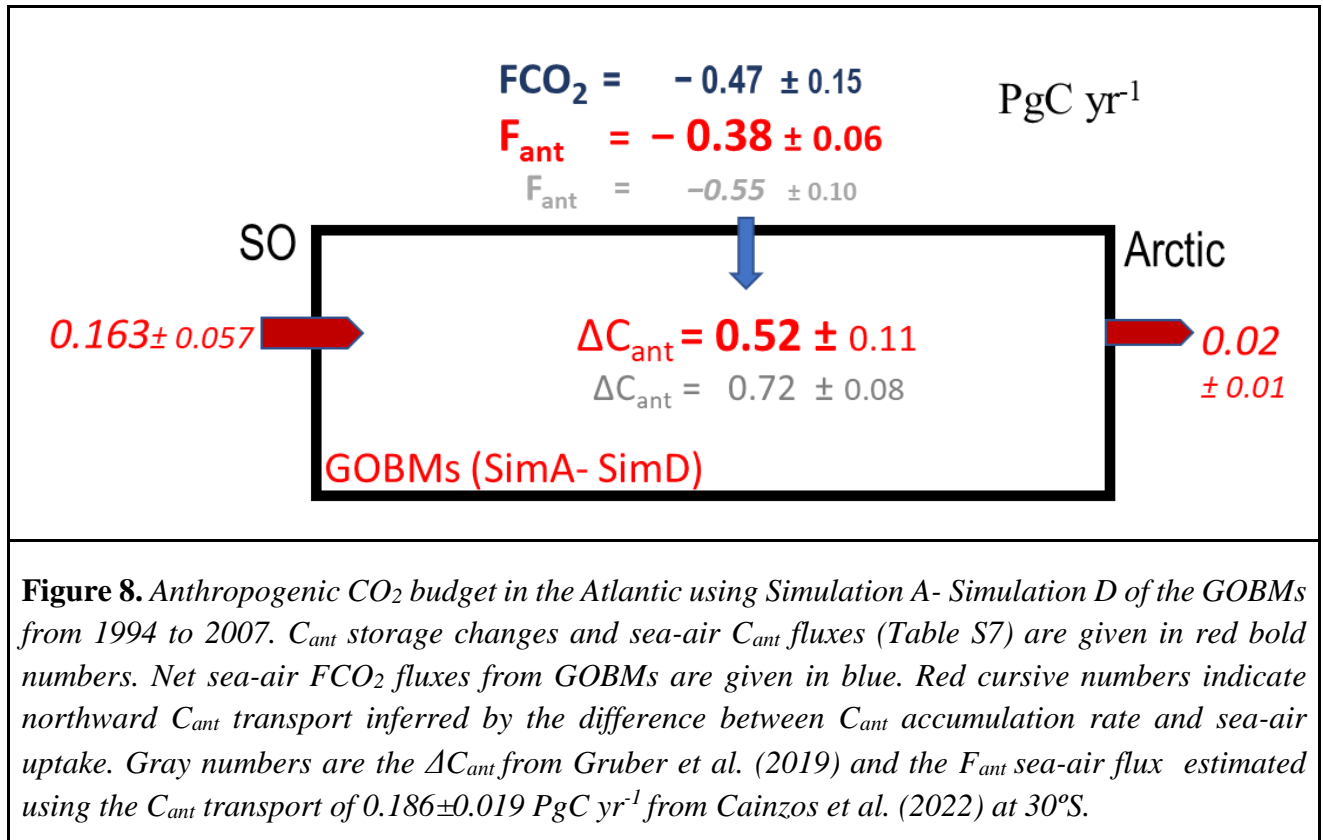
700 Knowing the accumulation rate of C_{ant} in the ocean interior and the flux entering from the
 701 atmosphere, we can infer horizontal transport rates (Figures 8 and S11). Given the enclosed
 702 bathymetry of the Mediterranean Sea, the GOBMs ensemble simulates a mean net export of C_{ant}
 703 from the Atlantic to the Mediterranean of $0.0055 \pm 0.0050 \text{ PgC yr}^{-1}$, inferred as the residual
 704 between an accumulation rate of $0.018 \text{ PgC yr}^{-1}$ and C_{ant} uptake from the atmosphere at a rate of
 705 $-0.012 \text{ PgC yr}^{-1}$ (Figure S11). This inferred C_{ant} import to the Mediterranean Sea is consistent with
 706 the observation-based transport estimates in the Strait of Gibraltar of $0.0042 \pm 0.0010 \text{ PgC yr}^{-1}$
 707 (Huertas et al., 2009).

708 From estimates of the exchange between the Nordic Seas and the Arctic (Jeansson et al.,
 709 2011) and the exchange from the Nares Strait, a net flux to the Arctic of $0.02 \pm 0.01 \text{ PgC yr}^{-1}$ was
 710 estimated. With this, the remaining lateral transport rates between the different biomes were
 711 estimated for each GOBM as the difference between surface flux, interior accumulation and the
 712 boundary fluxes. From the average of the GOBMs results (lateral C_{ant} transport and F_{ant} , Figure
 713 S11), the average transport from the Southern Ocean is obtained (Figures 8).

714 For the Atlantic, the northward transport of C_{ant} from the Southern Ocean decreases
 715 northward to almost zero (Figure S11) or reverses sign at the boundary between the NA STSS and
 716 NA SPSS biomes. These C_{ant} transports are fully compatible with the AMOC, in which the upper
 717 branch transports more C_{ant} northward than the southward lower branch, and also with the decrease
 718 of the vertical gradient of C_{ant} northward such that in the NA SPSS biome the vertical gradient of
 719 C_{ant} is small (Figure S10). With these results, the net transports of $0.163 \pm 0.057 \text{ PgC yr}^{-1}$ at the
 720 South Atlantic boundary obtained from the GOBM results are consistent with recent transports
 721 estimated from ocean sections at 30°S of $0.186 \pm 0.019 \text{ PgC yr}^{-1}$ (Cainzos et al., 2022). This suggests
 722 that the weak anthropogenic sea-air CO₂ fluxes are the primary cause of low C_{ant} accumulation
 723 rates in the South Atlantic. Although the total FCO₂ obtained from GOBMs are stronger in the

724 Atlantic than those derived from pCO₂ products, the lower C_{ant} accumulation rates in the interior
 725 ocean and in particular in the NA STPS and SA STPS biomes suggest that the anthropogenic
 726 contribution to the total FCO₂ in GOBMs is 30% weaker than expected from C_{ant} observations in
 727 the interior ocean.

728



729

730 The inferred northward C_{ant} transport at the southern boundary between Atlantic and
 731 Southern Oceans obtained for each of the nine GOBMs with Simulations A and D shows a high
 732 correlation (r²=0.61; p-level<0.01) with the maximum AMOC values at 26°N of each of these
 733 GOBMs (Figure S12), indicating that the northward physical transport is the main driver of the
 734 northward C_{ant} transport. We note additionally that, in comparison with observations, the GOBMs
 735 tend to underestimate the maximum AMOC values at 26°N (Figure S12) and hence the inferred
 736 northward C_{ant} transport.

737

738 4. Discussion

739 4.1 Progress since RECCAP1

740 With RECCAP2, we have updated estimates of the Atlantic Ocean CO₂ uptake (Figures 1 and 2;
 741 Table 1) using surface ocean pCO₂-observation based data products (pCO₂ products) and global

742 ocean biogeochemical models (GOBMs). The previous estimate made in RECCAP1 has a different
743 regional domain (spanning from 44°S to 79°N), and now the zonal region from 35°S to 44°S is no
744 longer part of the Atlantic Ocean but considered in the Southern Ocean mask (Hauck et al.,
745 submitted). In addition, the time period covered in RECCAP1 extends from 1990-2009, while it
746 extends from 1985 to 2018 in RECCAP2, even considering two sub-periods (before and after
747 2000). Moreover, an estimate of RCO flux component ($0.17 \pm 0.04 \text{ PgC yr}^{-1}$) was subtracted from
748 the values obtained for GOBMs in RECCAP1 (see Table S8 for details), not performed in
749 RECCAP2. However, to allow a direct comparison with RECCAP1 (Table S8), we added to
750 RECCAP2 Atlantic FCO₂ averages the values obtained for the zonal Atlantic region from 35°S to
751 44°S, characterized by high CO₂ uptake rates ($2.0 \pm 0.2 \text{ mol-C m}^{-2} \text{ yr}^{-1}$). Then, we brought the
752 regionally extended FCO₂ to the RECCAP1 time period. Our inferred RECCAP2-results for the
753 FCO₂ averages are similar to those published in RECCAP1 (Schuster et al., 2013) but with a slight
754 increase (Table S8), both in the GOBMs ensemble mean (21% increase) and pCO₂ products
755 ensemble average (9% increase).

756 Over the last decade, the nature of the pCO₂ products have changed significantly, not only
757 because of a significant growth in the number of observations (Bakker et al., 2016) but also because
758 of the implementation of new data interpolation methodologies (Rödenbeck et al., 2015, Denvil-
759 Sommer et al., 2019; Gregor et al., 2019). Nevertheless, the climatology of Takahashi et al. (2009),
760 which formed a cornerstone of the RECCAP1 studies, has proven to be a very robust product, with
761 estimates close to those obtained from the new pCO₂ products. On the modeling side, there have
762 also been many relevant advances between RECCAP1 and RECCAP2. In RECCAP1, only six
763 models were used while RECCAP2 employs almost twice the number of models, but yet both
764 model generations obtain similar results. The newly available GOBMs of RECCAP2 have been
765 improved in both physical and biological processes (e.g., Aumont et al., 2015; Schwinger et al.,
766 2016; Wright et al., 2021), and have an enhanced spatial resolution. With the advent of a variety
767 of mapping methods and comparable ensemble sizes of GOBMs and pCO₂-products, their
768 estimated air-sea CO₂ flux variability has become more similar (Crisp et al., 2022) although the
769 simulated interannual variability in the GOBMs on biome-scale is still lower than estimates based
770 on pCO₂ observation-based estimates (LeQuere et al., 2018; DeVries et al., submitted).

771 In terms of FCO₂ seasonality, the southern subtropical regions, the equatorial region and
772 northern subtropics studied in RECCAP1 followed the seasonal increase and decrease of pCO₂
773 driven mainly by warming and cooling. In the NA SPSS, the RECCAP1 pCO₂ products showed
774 that the seasonal cycle is reversed with a minimum during summer and outgassing in winter
775 (Schuster et al., 2013), conforming to direct observations (Olsen et al., 2008) whereas the seasonal
776 cycle of GOBMs was dominated by the temperature component. These general results remain
777 consistent in our analysis.

778 For the IAV in FCO₂, Schuster et al. (2013) found in RECCAP1 significant but weak
779 correlations to the NAO for the Equatorial biome with opposing signs between GOBMs ($r=-0.43$)
780 and pCO₂-products ($r=0.35$), potentially relating to their IAV being driven by SST-variations and

781 DIC-variations, respectively. Here, the new definition of the Equatorial biome in RECCAP2 helps
782 to confine the upwelling region such that the IAV in this region is DIC driven in both GOBMs and
783 pCO₂ products, with correlations of $r=-0.40$ and $r=-0.47$ with the NAO, respectively. In our case,
784 negative correlations indicate DIC-driven variations as we correlate the NAO with the sea-to-air
785 flux, while Schuster et al. (2013) correlated it with the air-to-sea flux (i.e. flux of opposite sign).
786 Yet, the issue of the GOBMs being more SST-driven remains also within the IAV of RECCAP2;
787 most notably in the North Atlantic subpolar gyre.

788 Even though RECCAP2 benefits from a substantial increase in observations and
789 improvements in modeling (complexity and resolution), the observed discrepancies in the seasonal
790 cycle between pCO₂ products and GOBMs in the NA SPSS are very similar to those described in
791 RECCAP1. Similar results were also obtained in the rest of the biomes with a comparable total
792 flux in the Atlantic. However, the averages of the pCO₂ products and GOBMs ensembles agree in
793 many key aspects, such as the average and the spatial distribution of the sink (Figure 1), but there
794 are still divergences in the magnitude and, above all, in decadal trends (Figure 3).

795

796 *4.2 The influence of the riverine CO₂ outgassing on comparisons of the CO₂ sink in* 797 *RECCAP2 models and observation-based products*

798

799 When averaged over the 1985 to 2018 period, the mean FCO₂ of pCO₂ products and
800 GOBMs ensembles agree within the ranges of their ensemble spread for most of the biomes and
801 the Atlantic basin (Table 1). The related spatial distribution of FCO₂ also agrees with respect to
802 the large-scale, basin-wide patterns (Figure 1), although some discrepancies are detected in the
803 NA SPSS biome. The average Atlantic FCO₂ estimated by the GOBMs ensemble is 30% lower
804 (i.e. an overestimation of the sink) than the estimate from pCO₂ products.

805 The riverine carbon outgassing (RCO, see Methods 2.4) hampers the comparison of the
806 FCO₂ estimates from the GOBMs with those of pCO₂ products, since the input of riverine carbon
807 and the burial of carbon is treated in various ways across the ensemble of GOBMs. Furthermore,
808 relevant output from the GOBMs is missing to properly assess the contribution of carbon,
809 alkalinity and nutrient input from land and their burial in sediments, resulting in a situation where
810 only a rough approximation of the RCO in the GOBMs is possible (Terhaar et al., submitted). In
811 the RECCAP2 protocol, it was recommended to apply the spatial distribution of the RCO of
812 Lacroix et al, (2020), scaled to a globally integrated RCO value of $0.65 \pm 0.3 \text{ PgC yr}^{-1}$ (Regnier et
813 al., 2022). This procedure results in a large adjustment of $0.27 \pm 0.06 \text{ PgC yr}^{-1}$ ($3.9 \pm 1.0 \text{ mol C m}^{-2}$
814 yr^{-1}) for the Atlantic sea-air CO₂ flux, which is more than half of the FCO₂ derived from the set of
815 GOBMs and 70% of that estimated from pCO₂ products (in absolute numbers). Although other
816 estimates of the RCO reported by Aumont et al. (2001) and Jacobson et al. (2007) reduce the RCO
817 in the Atlantic by 1/3, the relative magnitude of the RCO compared to the FCO₂ from GOBMs and
818 pCO₂ products remains substantial.

819 In the Atlantic Ocean the difference between the FCO_2 obtained by the ensemble pCO_2
 820 products and the ensemble of GOBMs is $0.10 \pm 0.11 \text{ PgC yr}^{-1}$. The RCO derived from Aumont et
 821 al. (2001), Jacobson et al. (2007), and Lacroix et al. (2020) scaled up to Regnier et al. (2022) are
 822 0.16 ± 0.05 , 0.16 ± 0.04 , and $0.27 \pm 0.06 \text{ PgC yr}^{-1}$, respectively (Table S3), yielding an ensemble
 823 average of $0.20 \pm 0.05 \text{ PgC yr}^{-1}$. All four of these values are higher than the average difference
 824 between the pCO_2 products and GOBMs, although within the combined uncertainty of all
 825 estimates. Importantly, for four of the five biomes (NA SPSS, NA STSS, AEQU and SA STPS),
 826 the ensemble RCO-estimates agree well with the FCO_2 differences (pCO_2 products minus
 827 GOBMs) with a mean difference of only $-0.001 \pm 0.019 \text{ PgC yr}^{-1}$ when the ensemble of RCO is
 828 added to the GOBMs estimate (last column in Table S3).

829 The biome with the largest discrepancy between FCO_2 in the GOBMs and in the pCO_2
 830 products is the NA STPS. Likewise, the three estimates of the RCO diverge most in this biome,
 831 indicating a high RCO-uncertainty. The FCO_2 difference between pCO_2 -products and GOBMs
 832 would require an RCO of $-0.024 \pm 0.013 \text{ PgC yr}^{-1}$ to be balanced, i.e., an additional CO_2 uptake
 833 rather than outgassing due to riverine input of carbon. However, this apparent RCO is of reversed
 834 sign and much lower than the ensemble mean of the direct RCO estimates ($+0.073 \pm 0.048 \text{ PgC yr}^{-1}$,
 835 Table S3). This discrepancy would even be larger when only the RCO estimate recommended
 836 in RECCAP2 ($+0.126 \pm 0.010 \text{ PgC yr}^{-1}$) would be used. At the same time, the C_{ant} accumulation
 837 rates (Table 1) and F_{ant} rates of the GOBMs in the NA STPS biome are lower than an observation-
 838 based estimate from Zunino et al. (2015), who used DIC measurements along the 26.5°N and 7.5°N
 839 sections from 1992/93 and 2010/11, and inferred a F_{ant} of $-0.23 \pm 0.02 \text{ PgC yr}^{-1}$ over an area of
 840 $15.3 \times 10^{12} \text{ m}^2$ (70% of NA STPS), which is more than twice the estimated F_{ant} in the GOBMs ($-$
 841 $0.084 \pm 0.010 \text{ PgC yr}^{-1}$, Figure S11). The F_{ant} difference between the GOBMs and the observation-
 842 based estimate from Zunino et al. is very similar to the difference between the direct RCO estimate
 843 ($+0.126 \pm 0.040 \text{ PgC yr}^{-1}$) and the apparent RCO ($-0.024 \pm 0.013 \text{ PgC yr}^{-1}$), which we inferred as
 844 the residual between the FCO_2 from pCO_2 -products and GOBMs. This agreement in the
 845 differences suggests that the GOBMs indeed underestimate the C_{ant} uptake in the NA STPS biome.
 846 If the GOBMs simulated a substantially stronger C_{ant} uptake (by about -0.1 PgC yr^{-1}), then the
 847 direct RCO estimate would plausibly explain the FCO_2 difference between the GOBMs and pCO_2
 848 products, albeit its large uncertainty. The likely underestimation of F_{ant} by the GOBMs in the NA
 849 STPS biome is further supported by their C_{ant} accumulation that is only about half as large as the
 850 observation-based estimate from Gruber et al. 2019 (Table 1), as well as the lower northward C_{ant}
 851 transport compared to two observation-based estimates (Brown et al. 2021; Cainzos et al. 2022).

852

853 *4.3 Temporal variability in sea-air CO_2 fluxes in models and pCO_2 products*

854 In the results-section, differences are discussed between models and pCO_2 products in sea-air CO_2 -
 855 flux dynamics in terms of trends, seasonality and interannual variability. The region where the
 856 GOBMs and pCO_2 products show the largest discrepancies is the NA SPSS; the biome with the
 857 highest CO_2 uptake rates. When looking at the seasonal decomposition of surface pCO_2 , it becomes

858 clear that the seasonality is primarily temperature driven in the GOBMs so that their CO₂ uptake
859 is larger in winter than in summer because of the seasonal SST changes. The seasonal cycle of the
860 pCO₂ products is driven by DIC-variations (for more information see Figure S4 and Rodgers et
861 al., in review). In the North Atlantic subpolar gyre, direct observations of interannual variability
862 in winter pCO₂ have shown that this is associated with variations in mixed layer depths in this
863 season (Fröb et al., 2019). That means that more intense mixing during colder winters leads to
864 higher surface DIC and consequently pCO₂, and thus a reduced flux of CO₂ into the ocean. A DIC-
865 driven dynamic is supported by the seasonal cycle of the pCO₂ products and the rather strong,
866 negative correlation of the pCO₂ product between the IAV of CO₂ flux and SST in this region
867 (Figure S8a). On the other hand, the GOBMs simulate positive correlations between IAV of CO₂
868 flux and SST. Hence the disagreement between pCO₂ products and GOBMs in IAV and seasonal
869 cycle is interconnected and driven by the same cause: SST-driven temporal variations in the
870 GOBMs versus DIC-driven temporal variations in the pCO₂-products. We note that the NA SPSS
871 is also the region in which pCO₂ products and GOBMs have the largest disagreement in their mean
872 CO₂-fluxes and the largest uncertainty in their CO₂-trends (see Figures 1 and 4).

873 When looking for the underlying causes for the disagreement in seasonal driving forces
874 and IAV between pCO₂ products and GOBMs in the NA SPSS, we find that most of the GOBMs
875 for which the simulated AMOC is available show significant correlations between their IAV of
876 CO₂ fluxes in the NA SPSS and AMOC-variations with correlation between 0.37 and 0.62.
877 Further, using Earth System Models, Goris et al. (2023) showed that the AMOC-strength drives
878 the simulated seasonal variability in the North Atlantic (Goris et al., 2023). Altogether, this
879 suggests that the underestimation of the AMOC in the GOBMs (Terhaar et al., submitted) could
880 be an underlying cause for the underestimation of the role of biogeochemical variability for both
881 IAV and seasonality by the GOBMs in the NA SPSS.

882 Furthermore, we identify that the comparatively small DIC-variations (as seen in both
883 seasonal cycle and IAV) in the GOBMs might also be a consequence of their current simplified
884 set-up, or the total lack, of riverine carbon fluxes (Terhaar et al., submitted). According to Aumont
885 et al. (2001) and Gao et al. (2023), the contribution of RCO weakens the CO₂ uptake in the NA
886 subpolar gyre and in the Southern Ocean. In fact, applying the predicted riverine carbon outgassing
887 of Aumont et al. (2001) to the NA SPSS biome removes the difference in FCO₂ mean fluxes (1985-
888 2018) between pCO₂ products and GOBMs (Table S3). The RCO modeled by Aumont et al. (2001)
889 also shows a similarity (in numbers) to the mean FCO₂ differences (1985-2018) between GOBMs
890 and pCO₂ products in the NA STSS, AEQU and SA STPS biomes (Table S3). The study of
891 Aumont et al. (2001) highlights the importance of the slow reactivity of dissolved organic carbon
892 (DOC) supplied by rivers to the regional distribution of CO₂-fluxes, which hence might also be
893 contributing significantly to seasonal and interannual variability.

894 Finally, the different strengths of drivers and the resulting large disagreements in IAV between
895 GOBMs and pCO₂ products may leave an imprint on the calculated trends of the sea-air CO₂-
896 fluxes of the NA SPSS biome for the period 2001-2018 (Figure 4). Here, the pCO₂ products show

897 an accelerated trend for the period 2001-2018 which is not simulated by the GOBMs. Similarly,
898 the IAV of the pCO₂ products is in a positive phase in the year 2000 and in a negative phase in the
899 year 2018 in the NA SPSS (Figure 6), which is not the case for the GOBMs. While this behavior
900 is especially pronounced in the NA SPSS, the NA STPS biome shows a similar phasing in their
901 IAV when comparing GOBMS and pCO₂ products. In a previous study (McKinley et al., 2020) it
902 has been found that the IAV is a potential driver of differences in trends between observational
903 products and GOBMs.

904 While the IAV has an influence on the decadal trends, it cannot solely explain that the
905 calculated trends of sea-air CO₂ fluxes before and after the year 2000 are similar across our
906 ensemble of GOBMs, while the trends obtained from surface CO₂ observations show a sharp
907 increase between the trend of the pre-2000 and post-2000. We advise caution when comparing the
908 CO₂ trends before the year 2000 between GOBMs and pCO₂-products, as the trends of the pCO₂
909 products is strongly conditioned by the FCO₂ estimates in the early years (Figure S2), where the
910 available observations (pCO₂ data and predictors) to generate the pCO₂ products are far less, such
911 that the estimates of the pCO₂ products agree less than in later years (Figures 3 and S2). In fact,
912 the pCO₂ products do not agree on the CO₂ trends before the year 2000 (-0.024 ± 0.075 PgC-yr⁻¹
913 dec⁻¹) with three pCO₂ products suggesting a weakening of the CO₂ uptake in the Atlantic before
914 2000 and four pCO₂ products a strengthening (Table S5). For the trends after the year 2000, the
915 agreement of the pCO₂ products allows for a more confident estimate of a strengthening CO₂ sink
916 in the Atlantic with a trend of -0.126 ± 0.031 PgC-yr⁻¹ dec⁻¹, which is twice the trend estimated by
917 the GOBMs, of -0.060 ± 0.017 PgC-yr⁻¹ dec⁻¹. Nevertheless, for one of the pCO₂-products (MPI-
918 SOM-FFN) it has been shown that an ideal sampling strategy would reduce the trend estimate in
919 the northern hemisphere for the years 2000-2018 (Hauck et al., 2023). Hence, a skewed sampling
920 strategy could potentially influence the 2000-2018 trend estimate of the pCO₂-products. For the
921 GOBMs, we want to note that their simulated seasonal cycle might lead to a trend estimate that is
922 too low, as it has been shown for an ensemble of Earth System Models that a more SST-driven
923 seasonal cycle is related to shallower MLD and a less vivid AMOC (Goris et al., 2018). Earth
924 System Models with a weaker AMOC simulate more warming and less future carbon uptake in
925 the North Atlantic. Contrarily, a biology-driven seasonal cycle will lead to enhanced carbon uptake
926 due to the increasing sensitivity of pCO₂ to DIC-variations with declining buffer capacity of the
927 ocean (Hauck et al., 2015).

928

929 *4.4 C_{ant} Storage and transport*

930 In the Atlantic, the GOBMs ensemble underestimates the C_{ant} accumulation rate (1994-
931 2007) by $28 \pm 20\%$ relative to the estimate of Gruber et al. (2019), which is possibly related to a
932 combination of physical, chemical and methodological factors. In general, both GOBMs and the
933 Gruber et al. (2019) product show maximum C_{ant} concentrations near the surface with a rapid
934 decrease towards depth. Nevertheless, surface GOBM estimates are always slightly lower than the
935 observation-based product, which might be related to biases in the Revelle factor caused by too

936 high preindustrial CO₂ values in a couple of GOBMs with a late starting date past 1765 (Terhaar
937 et al., submitted). The highest agreement between GOBMs and the observation-based product in
938 ΔC_{ant} is found north of 30°N, while the GOBMs simulate systematically lower accumulation rates
939 in the South Atlantic (Figure 7, Table 1). In the upper ocean layer, where the upper limb of the
940 AMOC is located, the differences in ΔC_{ant} are not particularly evident (Fig. S10). However,
941 between 1400 and 3000 m depths, GOBMs do not reproduce the C_{ant} peak estimated by the
942 observation-based product (Rhein et al. 2015; Rios et al. 2012; Fajar et al. 2015, Gruber et al.
943 2019) for the Atlantic (Figure S10) and, more specifically, for the NA STPS, AEQU and SA STPS
944 biomes. This depth interval, with lower C_{ant} by GOBMs compared to the observation-based
945 estimate, coincides with the depth at which the NADW is located. This result suggests that over
946 the 1994–2007 period the GOBMs simulated too little C_{ant} advection into the South Atlantic within
947 the Deep Western Boundary Current that carries the C_{ant} -rich NADW towards the Southern
948 hemisphere (Goris et al., 2023). This result is consistent with the fact that most of the RECCAP2
949 GOBMs simulate too weak AMOC strengths (Terhaar et al., submitted). In addition, we note that
950 biased low C_{ant} uptake in the Southern Ocean (Hauck et al., submitted), and the subsequent
951 northward transport to the Atlantic, could also contribute to the too-low C_{ant} accumulation rate in
952 the South Atlantic by GOBMs. However, the transport of C_{ant} from the Southern Ocean to the
953 Atlantic is in accordance with the observations (Cainzos et al., 2022). We also note that the GOBMs
954 may underestimate the temporal variability of the ocean interior transport, since the C_{ant}
955 accumulation rates of the GOBMs in the South Atlantic are more similar to the estimates by
956 Khatiwala et al. (2009), which assumes a quasi-stationary ocean circulation (see Table 1 for SA
957 STPS biome). In contrast, the GOBMs show a lower decadal variability of the C_{ant} accumulation
958 rates than observation-based products (Gruber et al. 2019; Müller et al., in press). The interannual
959 variability of the C_{ant} accumulation rates, derived from the linear regressions, is typically $1.5 \pm 1.0\%$
960 of the absolute rates across all biomes and the whole Atlantic Ocean, indicating that the C_{ant}
961 accumulation in the GOBMs occurs as a rather steady process.

962 The assessment of C_{ant} accumulation and transport in the Atlantic conducted in RECCAP1
963 (Khatiwala et al., 2013) revealed that the largest anthropogenic CO₂ uptake occurs in the Southern
964 Ocean, with much of this uptake being transported equatorward through the Antarctic Intermediate
965 Water and Subantarctic Mode Water. Most of this C_{ant} is stored in the SA STPS (Mikaloff Fletcher
966 et al., 2006). There is also a significant C_{ant} uptake in the tropical Atlantic that is partially
967 transported southward, but most of it is stored in the tropics or transported northward. The C_{ant}
968 taken up in the North Atlantic is transported northward in the upper limb of the AMOC and
969 subsequently entrained to the NADW and transported southward in the lower limb of AMOC. The
970 GOBMs analyzed here confirm these spatial patterns of C_{ant} accumulation (though accumulation
971 is low in the South Atlantic below 1500 m, Figures 7, S9, and S10) and of meridional transport
972 (dominated by inflow from the Southern Ocean, Figures 8 and S11).

973 Khatiwala et al., (2013) stated that the C_{ant} transports estimated from GO-SHIP sections using
974 hydrographic data and observation-based C_{ant} estimates (Holfort et al., 1998; Álvarez et al., 2003;
975 Macdonald et al., 2003; Rosón et al., 2003; Pérez et al., 2013) represent C_{ant} transport at a single

976 time point. Such C_{ant} transport estimates may be biased because seasonal variability is not resolved
977 (Wilkin et al., 1995). However, recent estimates cover long time series (Brown et al., 2021), or
978 aim to provide decadal climatological estimates (Cainzos et al., 2022). In RECCAP1, Khatiwala
979 et al. (2013) showed that C_{ant} transports, obtained based on GOBMs and from hydrographic
980 sections, exhibit similar C_{ant} transports between 44°S and the Equator with a northward transport
981 of 0.15 to 0.20 PgC yr⁻¹, but, in contrast, in the North Atlantic the GOBMs simulated a gradual
982 northward decrease of the C_{ant} transport, reaching zero horizontal net transport between 35° and
983 60°N. This pattern is confirmed in RECCAP2 (Figure S11) with a larger number of GOBMs
984 involved. Estimates of transport in the 26°N along transoceanic sections (Macdonald et al., 2003;
985 Rosón et al., 2003; Perez et al., 2013; Zunino et al. 2015; Brown et al, 2021; Cainzos et al., 2022)
986 showed larger values than those of the oceanic inversion or GOBMs. These discrepancies
987 remained uncertain in RECCAP1 due to the uncertainties in the hydrographic estimates and the
988 difficulties in directly comparing the two techniques. However, one must also consider the
989 difficulties that inverse models and GOBMs have in representing mesoscale processes, mainly in
990 regions of very intense currents such as the Florida Current, Gulf Stream, and DWBC (Khatiwala
991 et al. 2013, Hirschi et al. 2020; Ma et al., 2016; Bower et al. 2019).

992 Recent estimates by Brown et al. (2021) using the RAPID long time series (2004-2012),
993 with an assessment of C_{ant} transports at 10-day timescale, confirm a strong C_{ant} transport at 26.5°N
994 of 0.191 ± 0.013 PgC yr⁻¹, which is in the middle of the range (0.128 ± 0.032 to 0.25 ± 0.05 PgC yr⁻¹)
995 of the eight estimates obtained from five sections between 1992 and 2011 (collected in Cainzos et
996 al., 2022). The ensemble average C_{ant} transport over 26°N obtained for the nine GOBMs used here
997 is 0.053 ± 0.037 PgC yr⁻¹, which is almost four times lower than the C_{ant} transport of Brown et al.
998 (2021). Racapé et al. (2018), using a global NEMO-PISCES model with a finer spatial resolution
999 ($0.5^\circ \times 0.5^\circ$), obtained a northward transport of 0.092 ± 0.04 PgC yr⁻¹ somewhat closer to
1000 observation-based estimates, suggesting that the spatial resolution of the GOBMs is relevant for
1001 the simulation of ocean interior transport. Observational-based evaluations of C_{ant} transport
1002 indicate the dynamical difficulties that CMIP5/6 climate models in certain regions have in
1003 achieving realistic projections of the AMOC and DWBC, when run at relatively coarse resolutions
1004 on the order of 1° (Hirschi et al., 2020; Ma et al., 2016), which does not allow to correctly simulate
1005 vertical structures nor to resolve mesoscale ocean eddies (Bower et al., 2019). For the RECCAP2
1006 GOBMs, it was shown that the AMOC is, on average, underestimated by 3.1 ± 5.2 Sv at 26.5°N,
1007 which can partly explain this discrepancy between GOBMs and pCO₂ products (Terhaar et al.,
1008 submitted).

1009 The weak C_{ant} northward transport in the subtropical region as shown by GOBMs might
1010 also be connected to a possible mismatch in C_{ant} uptake in the NA STPS biomes (Zunino et al.,
1011 2015) described above. Despite the agreement in mean FCO₂ between pCO₂-products and GOBMs
1012 in the NA STPS, the mismatch between the potentially strong RCO (Table S3) and the ‘residual
1013 RCO’ (difference between GOBMs and pCO₂-products) further supports that the GOBMs simulate
1014 a too low C_{ant} uptake (Table S3) despite the apparent agreement in the net flux. The reduced C_{ant}
1015 uptake would be conveyed both northward and downward to the ocean interior. In fact, Cainzos et

1016 al. (2022) show that the contribution of vertical mixing is somewhat larger than the southward
1017 horizontal advection into the accumulation of C_{ant} in the lower limb of AMOC. Therefore, the
1018 insufficient incorporation of the RCO in the GOBMs may also result in a lower CO_2 uptake, and
1019 at the same time also generates an excess CO_2 uptake in the NA SPSS (Aumont et al. 2001; Gao
1020 et al. 2023).

1021

1022 *4.5 Future recommendations*

1023 Observations of pCO_2 in the Atlantic Ocean have greatly improved over the past two
1024 decades making it one of the most densely sampled oceans temporally and spatially. However, the
1025 surface pCO_2 observations are highly skewed in space and time, potentially inducing spurious
1026 results in the gap-filling algorithms used for estimating CO_2 fluxes. In fact, even in the well
1027 sampled Atlantic, the observations cover less than 10% of all $1^\circ \times 1^\circ$ by 1 month grid points,
1028 requiring the gap filling methods to fill more than 90% of the grid cells. Recent studies with
1029 synthetic model data using similar resolution and parameterizations to observations (Gloege et al.,
1030 2021; Hauck et al., 2023) indicate that gap-filling methods may be prone to a possible
1031 overestimation of the decadal rates of increase in CO_2 uptake when data are sparse, partially
1032 explaining the discrepancy between these products and GOBMs. We also note that in the data-
1033 sparse period 1985-2000, the trends generated by the various observation-based products were
1034 highly correlated with their flux estimate in 1985. This shows that with reduced observational
1035 coverage, the trend in the products tends to drift apart. Therefore, data-coverage as well as gap-
1036 filling methods need to be improved to reduce uncertainties in the trends. It is now quite worrisome
1037 that key Atlantic ship of opportunity lines for surface ocean pCO_2 observations have been lost or
1038 operated with reduced capacity the past years - this tendency must be reversed if we want to retain
1039 our ability to accurately constrain the Atlantic Ocean CO_2 sink and its variability

1040 The Atlantic Ocean is characterized by high temporal dynamics not only in the surface
1041 layer but also in the deep layers connecting the North Atlantic to the Southern Ocean through the
1042 deep western boundary current. This involves strong mesoscale and sub-mesoscale dynamic
1043 currents and structures. The effectiveness of GOBMs in representing dynamic climate change
1044 processes is highly dependent on their spatial and temporal resolutions. Current spatial resolution
1045 can barely reproduce the dynamics of strong CO_2 transports in the Atlantic, as well as ocean-
1046 coastal interactions.

1047 A number of future model improvements could further address or minimize the
1048 discrepancies in the interior C_{ant} inventory estimates. As simulations of the ocean biogeochemistry
1049 are strongly constrained by the performance of the physical model (Doney et al., 2004), more
1050 detailed assessments of key physical dynamics that govern the surface to deep carbon transport
1051 such as the representation of mode water, intermediate and deep waters in the North Atlantic
1052 should be carried out (Racape et al., 2018). Assessment of GOBMs' ability to simulate observed
1053 episodic ventilation events and their impact on interior C_{ant} , e.g., as documented in Rhein et al.
1054 (2017) and Fröb et al. (2016), could shed additional light on their validity. Through winter

1055 convective mixing, biases in the interior carbon chemistry can influence the upper ocean carbon
1056 uptake capacity in models due to biases in the buffering capacity of the ocean (Vaittinada Ayar et
1057 al., 2022; Terhaar et al., 2022). Improvements in the representation of mixing by the models would
1058 likely also alleviate the issues with the simulated amplitude and timing of spring bloom and winter
1059 remineralization in the subpolar region (that we identified as key deficiencies in GOBMs) and
1060 further improve their FCO₂ seasonal cycle. Better observational constraints and improvement in
1061 mixing parameterizations are needed to alleviate this issue. Higher spatial resolution is likely
1062 necessary to improve key upper ocean physical features in the Atlantic Ocean such as the Gulf
1063 Stream, which has been shown to play a significant role in constraining the seasonality and trends
1064 of North Atlantic carbon fluxes and interior sequestration (Chassignet et al., 2020; Goris et al.,
1065 2023). Results from the high-resolution regional model (ROMS-ETHZ) indicate a better
1066 representation of the FCO₂ seasonal cycle in the NA SPSS and a better representation of the trends
1067 for 2001-2018 in NA SPSS, NA STSS and SA STPS, while we see no improvement or even a
1068 worse representation in other regions. A detailed and overarching investigation of the benefits of
1069 higher resolution for the carbon cycle would be desirable. Further, as the number of observations
1070 continue to increase, improvements in biogeochemical parameterizations can be achieved through
1071 data assimilation, e.g. to address the regionally heterogeneous biological processes (Tjiputra et al.,
1072 2007; Gharamti et al., 2017). In addition, improvement in biological model complexity may be
1073 needed to optimally reproduce the observed biogeochemical dynamics across spatially varying
1074 regimes such as the Atlantic basin (Gehlen et al., 2015). Finally, the interior lateral transport of
1075 C_{ant} is projected to play an increasing role in the future (Tjiputra et al., 2010). Better constraints of
1076 the northward (and southward) transport of anthropogenic CO₂ in the ocean, through the upper
1077 (and lower) limb of the AMOC should be considered to improve estimates of fluxes further north
1078 (Cainzos et al., 2022). Finally, an improved model experiment protocol that includes a multi-
1079 centennial preindustrial spin up (Seferian et al., 2016), common initialization procedure, and
1080 implementation of the river carbon loop should be considered (see also Terhaar et al., submitted).

1081 In the North Atlantic, Fontela et al., (2020) showed that semi-refractory DOC
1082 mineralization in the lower limb of AMOC represents a significant contribution to DIC of the same
1083 order of magnitude as CO₂ exchange with the atmosphere, resulting in a possible CO₂ source that
1084 will fit with the differences observed between the observed FCO₂ (Takahashi et al., 2009) and
1085 those estimated by inverse methods (Mikaloff Fletcher et al., 2007; Gruber et al., 2009; Gerber et
1086 al., 2009). In RECCAP, the role that DOC has not been evaluated and DOC cycle can play both
1087 at the seasonal cycle level, i.e. diverting DIC which reduces pCO₂ in summer or by DOC deep
1088 mineralization, increasing DIC transport. The semi-refractory DOC is exported to the mesopelagic
1089 zone and even deeper depths in the North Atlantic, as documented by Hansell (2013). He has
1090 assessed in ~0.34 PgC yr⁻¹ DOC export with a mineralization time scale to CO₂ of decades. In the
1091 North Atlantic the coupling between DOC production and export is revealed in the export of
1092 locally produced DOC (Roshan and DeVries, 2017; Fernandez-Castro et al., 2019). In fact, the
1093 carbon sequestration mediated by DOC represents around a third of the North Atlantic CO₂ sink
1094 (Fontela et al., 2016). It has been demonstrated in DOC enrichment along the AMOC and its

1095 coupling with intense overturning in the NA SPSS leads to downward transport of 0.07 PgC yr^{-1}
1096 associated mainly with water masses transported by the DWBC (Fontela et al., 2020). In addition,
1097 0.09 PgC yr^{-1} of DOC exported northward from the subtropics is mineralized in the deep layers
1098 of the AMOC. Inverse models do not include the DOC divergence which is assumed to be small
1099 (Mikaloff Fletcher et al., 2007). This carbon cycle component has not been evaluated neither in
1100 RECCAP1 nor in RECCAP2 and, considering the importance of its magnitude relative to FCO_2 ,
1101 it is relevant to consider it in future biogeochemical modeling experiments together with other
1102 modeling improvements proposed here.

1103

1104 **5 Conclusions**

1105 We provide here the current "best estimate" of surface CO_2 fluxes as well as the
1106 accumulation and transport of C_{ant} in the Atlantic, including the Mediterranean Sea for the
1107 RECCAP2 period, 1985-2018. For this estimate, we have compared different types of ocean
1108 biogeochemical models (GOBMs, ROBMs, data-assimilated models) with various observation-
1109 based products. Our analysis includes several time-scales of variability.

1110 We find that the **mean** net sea-air CO_2 flux of the GOBMs ensemble is 27% stronger than
1111 estimates from observation-based pCO_2 products. This difference is within the uncertainties of the
1112 GOBMs and pCO_2 products and can be explained by known discrepancies between pCO_2 -products
1113 and GOBMs, including the oceanic CO_2 outgassing due to the impact of riverine discharge that is
1114 not explicitly represented in most GOBMs.

1115 The **trends** of sea-air CO_2 fluxes before and after year 2000 are similar across our ensemble
1116 of GOBMs (from -0.045 ± 0.012 to $-0.060 \pm 0.017 \text{ PgC-yr}^{-1} \text{ dec}^{-1}$) and are consistent with the 43%
1117 increase in the atmospheric CO_2 growth rate between the pre-2000 period and the post-2000
1118 period. In contrast, the trends obtained from surface CO_2 observations show a sharp increase from
1119 the trend of the pre-2000 of $-0.024 \pm 0.075 \text{ PgC-yr}^{-1} \text{ dec}^{-1}$ to a trend of $-0.126 \pm 0.031 \text{ PgC-yr}^{-1} \text{ dec}^{-1}$
1120 in the post-2000 period.

1121 All biomes apart from the subpolar North Atlantic show a high correlation between
1122 GOBMs and pCO_2 products in terms of FCO_2 seasonality. In the North Atlantic subpolar biome,
1123 the GOBMs simulate a seasonal cycle driven predominantly by temperature variation, which the
1124 pCO_2 -products do not show.

1125 Averaged over the Atlantic, the ensemble of GOBMs shows lower interannual variability
1126 (IAV) in FCO_2 than the pCO_2 products. Spatially, and temporally, pCO_2 products and GOBMs
1127 agree well in most of the Atlantic biomes but disagree quite substantially in the subpolar North
1128 Atlantic. Here, the variability of the GOBMs is mostly driven by SST variations, which is not the
1129 case for the pCO_2 products.

1130 The mean C_{ant} storage change between 1994-2007 simulated by the GOBMs ensemble was

1131 found to be 28% lower than that estimated from DIC observations in the ocean interior and 25%
1132 lower than the data-assimilated model. These differences are higher than the standard deviation of
1133 the GOBMs estimates (17%). In contrast to the results described for the surface CO₂ fluxes, there
1134 is high agreement in anthropogenic CO₂ storage rates between GOBMs and those based on DIC
1135 observations in the NA SPSS and NA STSS biomes, whereas there are significant differences in
1136 the NA STPS, AEQU and SA STPS biomes, where the GOBM-estimates are on average 36%
1137 lower than observation-based estimates. The GOBMs indicate that 32% of the C_{ant} stored in the
1138 Atlantic comes from the Southern Ocean, in line with previous estimates from the literature. The
1139 Mediterranean Sea revealed an almost balanced net air-sea flux of CO₂, however it presented a
1140 C_{ant} accumulation of 0.018 PgC yr⁻¹, of which 70% are taken up from the atmosphere and 30% are
1141 imported from the Atlantic.

1142 Estimates of the land-to-ocean transport of carbon and nutrients indicate a significant and
1143 large net CO₂ outgassing due to the input of this terrestrially derived matter. The protocol of
1144 RECCAP2 recommended the use of the updated estimate of 0.65 PgC yr⁻¹ of Regnier et al. (2022)
1145 at the global level. For the Atlantic Ocean, the outgassing rates per square meter are twice the
1146 global rates when considering the spatial distribution of the riverine carbon outgassing (RCO)
1147 simulated by Lacroix et al. (2020). This RCO is especially significant in the NA STPS biome and
1148 hampers the comparison of GOBM and observation-based estimates of CO₂ fluxes, transport and
1149 accumulation. Therefore, it is essential to have more realistic models to better understand the
1150 influences of land-sea fluxes in the Atlantic Ocean and to be able to use observational-estimates
1151 with confidence when determining the accumulation of C_{ant}.

1152

1153 **Acknowledgments**

1154 The authors have no conflicts of interest. F. F Pérez and A. Velo were supported by the
1155 BOCATS2 (PID2019-104279GB-C21) project funded by MCIN/AEI/10.13039/501100011033,
1156 and with E. Huertas contributed to WATER:iOS CSIC PTI. M. Becker acknowledges funding
1157 from the Research Council of Norway through N-ICOS-2 (grant no 296012), and Nansen Legacy,
1158 grant no. 276730. NGo was supported by the strategic project DYNASOR (DYnamics of the North
1159 Atlantic Surface and Overturning ciRculation) of the Bjerknes Centre for Climate Research. M.
1160 Lopez-Mozos was supported by the grant PRE2020-093138 funded by MCIN/AEI/
1161 10.13039/501100011033 and by “ESF Investing in your future”. J. Tjiputra acknowledges funding
1162 from EU funded H2020 projects TRIATLAS (no. 817578) and OceanICU (no. 101083922). A.
1163 Olsen appreciates support from the Research Council of Norway through N-ICOS-2 (grant no
1164 296012), and Horizon Europe through grant no. 101083922 (OceanICU Improving Carbon
1165 Understanding). J.D. Muller, and N. Gruber acknowledge support from the European Union's
1166 Horizon 2020 research and innovation program under grant agreement no. 821003 (project
1167 4C) and no. 820989 (project COMFORT). J. Hauck acknowledges funding from the Initiative and

1168 Networking Fund of the Helmholtz Association (Helmholtz Young Investigator Group Marine
1169 Carbon and Ecosystem Feedbacks in the Earth System [MarESys], grant number VH-NG-1301)
1170 and from ERC-2022-STG OceanPeak, grant agreement 101077209

1171

1172 **Open Research**

1173 All of the RECCAP2 data will be made available in a public repository before publication.

1174

1175 **References**

1176 Andri , C., Oudot, C., Genthon, C., & Merlivat, L. (1986), CO₂ fluxes in the tropical Atlantic
1177 during FOCAL cruises, *Journal of Geophysical Research*, 91(C10), 11741– 11755,
1178 <https://doi.org/10.1029/JC091iC10p11741>

1179  lvarez, M., R os, A. F., P erez, F. F., Bryden, H. L., & Ros n, G. (2003). Transports and
1180 budgets of total inorganic carbon in the subpolar and temperate North Atlantic. *Global*
1181 *Biogeochemical Cycles*, 17(1), 2-1. <https://doi.org/10.1029/2002GB001881>

1182 Aumont, O., Ethe, C., Tagliabue, A., Bopp, L., & Gehlen, M. (2015). PISCES-v2: an ocean
1183 biogeochemical model for carbon and ecosystem studies. *Geoscientific Model Development*, 8,
1184 2465-2513. <https://doi.org/10.5194/gmd-8-2465-2015>

1185 Aumont, O., Orr, J. C., Monfray, P., Ludwig, W., Amiotte-Suchet, P., & Probst, J.-L. (2001).
1186 Riverine-driven interhemispheric transport of carbon, *Global Biogeochemical Cycles*, 15(2),
1187 393–405. <https://doi.org/10.1029/1999GB001238>

1188 Bakker, D. C. E., Pfeil, B., Landa, C. S., Metzl, N., O’Brien, K. M., Olsen, A., et al. (2016). A
1189 multi-decade record of high-quality CO₂ data in version 3 of the Surface Ocean CO₂ Atlas
1190 (SOCAT). *Earth System Science Data*, 8, 383–413. <https://doi.org/10.5194/essd-8-383-2016>

1191 Bakker, D. C. E., Alin, S. R., Becker, M., Bittig, H., Casta o-Primo, R., Feely, R. A., et al.
1192 (2022). *SOCAT version 2022 for quantification of ocean CO₂ uptake*. Available at:
1193 https://www.socat.info/wp-content/uploads/2022/06/2022_Poster_SOCATv2022_release.pdf.

1194 Bates, N. R., Takahashi, T., Chipman, D. W., & Knap, A. H. (1998). Variability of pCO₂ on diel
1195 to seasonal timescales in the Sargasso Sea near Bermuda. *Journal of Geophysical Research:*
1196 *Oceans*, 103(C8), 15567-15585. <https://doi.org/10.1029/98JC00247>

1197 Bates, N. R., Astor, Y. M., Church, M. J., Currie, K., Dore, J. E., Gonz lez-D vila, M., ... &
1198 Santana-Casiano, J. M. (2014). A time-series view of changing surface ocean chemistry due to
1199 ocean uptake of anthropogenic CO₂ and ocean acidification. *Oceanography*, 27(1), 126-141.
1200 <http://www.jstor.org/stable/24862128>

1201 Becker, M., Steinhoff, T., & K rtzinger, A. (2018). A detailed view on the seasonality of stable
1202 carbon isotopes across the North Atlantic. *Global Biogeochemical Cycles*, 32, 1406– 1419.
1203 <https://doi.org/10.1029/2018GB005905>

1204 Bower, A., Lozier, S., Biastoch, A., Drouin, K., Foukal, N., Furey, H., ... & Zou, S. (2019).

- 1205 Lagrangian views of the pathways of the Atlantic Meridional Overturning Circulation. *Journal of*
 1206 *Geophysical Research: Oceans*, 124(8), 5313-5335. <https://doi.org/10.1029/2019JC015014>
- 1207 Brady, R. X., Lovenduski, N. S., Alexander, M. A., Jacox, M., & Gruber, N. (2019). On the role
 1208 of climate modes in modulating the air–sea CO₂ fluxes in eastern boundary upwelling systems.
 1209 *Biogeosciences*, 16, 329–346. <https://doi.org/10.5194/bg-16-329-2019>
- 1210 Breeden, M. L., & McKinley, G. A. (2016). Climate impacts on multidecadal pCO₂ variability
 1211 in the North Atlantic: 1948–2009. *Biogeosciences*, 13(11), 3387-3396.
 1212 <https://doi.org/10.5194/bg-13-3387-2016>
- 1213 Brown, P. J., McDonagh, E. L., Sanders, R., Watson, A. J., Wanninkhof, R., King, B. A., et al.
 1214 (2021). Circulation-driven variability of Atlantic anthropogenic carbon transports and uptake.
 1215 *Nature Geosciences*, 14, 571–577. <https://doi.org/10.1038/s41561-021-00774-5>
- 1216 Caínzos, V., Velo, A., Pérez, F. F., & Hernández-Guerra, A. (2022). Anthropogenic carbon
 1217 transport variability in the Atlantic Ocean over three decades. *Global Biogeochemical Cycles*,
 1218 36, e2022GB007475. <https://doi.org/10.1029/2022GB007475>
- 1219 Chassignet, E. P., Yeager, S. G., Fox-Kemper, B., Bozec, A., Castruccio, F., Danabasoglu, G., et
 1220 al. (2020). Impact of horizontal resolution on global ocean–sea ice model simulations based on
 1221 the experimental protocols of the Ocean Model Intercomparison Project phase 2 (OMIP-2).
 1222 *Geoscientific Model Development*, 13, 4595–4637. <https://doi.org/10.5194/gmd-13-4595-2020>
- 1223 Chau, T. T. T., Gehlen, M., & Chevallier, F. (2022). A seamless ensemble-based reconstruction
 1224 of surface ocean pCO₂ and air–sea CO₂ fluxes over the global coastal and open oceans.
 1225 *Biogeosciences*, 19 (4), 1087–1109. <https://doi.org/10.5194/bg-19-1087-2022>
- 1226 Clement, D., & Gruber, N. (2018). The eMLR (C*) method to determine decadal changes in the
 1227 global ocean storage of anthropogenic CO₂. *Global Biogeochemical Cycles*, 32(4), 654-
 1228 679. <https://doi.org/10.1002/2017GB005819>
- 1229 Coppola, L., Diamond Riquier, E., & Carval, T. (2018). Dyfamed Observatory Data. SEANOE.
 1230 <https://doi.org/10.17882/43749>.
- 1231 Crisp, D., Dolman, H., Tanhua, T., McKinley, G. A., Hauck, J., Bastos, A., ... & Aich, V. (2022).
 1232 How well do we understand the land-ocean-atmosphere carbon cycle?. *Reviews of Geophysics*,
 1233 60(2), e2021RG000736. <https://doi.org/10.1029/2021RG000736>
- 1234 Denvil-Sommer, A., Gehlen, M., Vrac, M., & Mejia, C. (2019). LSCE-FFNN-v1: a two-step
 1235 neural network model for the reconstruction of surface ocean pCO₂ over
 1236 the global ocean. *Geoscientific Model Development*, 12(5), 2091-2105.
 1237 <https://doi.org/10.5194/gmd-12-2091-2019>
- 1238 De Carlo, E. H., Mousseau, L., Passafiume, O., Drupp, P. S., and Gattuso, J.-P. (2013).
 1239 Carbonate chemistry and air–sea CO₂ flux in a NW Mediterranean Bay over a four-year period:
 1240 2007–2011. *Aquat. Geochem.* 19: 399–442. <https://doi.org/10.1007/s10498-013-9217-4>
- 1241 DeVries, T. (2014). The oceanic anthropogenic CO₂ sink: Storage, air-sea fluxes, and transports
 1242 over the industrial era. *Global Biogeochemical Cycles*, 28(7), 631-647.
 1243 <https://doi.org/10.1002/2013GB004739>
- 1244 DeVries, T. (2022). Atmospheric CO₂ and sea surface temperature variability cannot explain
 1245 recent decadal variability of the ocean CO₂ sink. *Geophysical Research Letters*, 49(7),

- 1246 e2021GL096018. <https://doi.org/10.1029/2021GL096018>
- 1247 DeVries, T., Yamamoto, K., Wanninkhof, R., Gruber, N., Hauck, J., Müller, J. D. et al.
 1248 (submitted). Magnitude, trends, and variability of the global ocean carbon sink from 1985-2018,
 1249 *Global Biogeochemical Cycles*.
- 1250 Doney, S. C., Lindsay, K., Caldeira, K., Campin, J.-M., Drange, H., Dutay, J.-C., et al. (2004).
 1251 Evaluating global ocean carbon models: The importance of realistic physics. *Global*
 1252 *Biogeochemical Cycles*, 18, GB3017. <https://doi.org/10.1029/2003GB002150>
- 1253 Fajar, N. M., Guallart, E. F., Steinfeldt, R., Ríos, A. F., Pelegrí, J. L., Pelejero, C., ... & Pérez, F.
 1254 F. (2015). Anthropogenic CO₂ changes in the equatorial Atlantic Ocean. *Progress in*
 1255 *Oceanography*, 134, 256-270. <https://doi.org/10.1016/j.pocean.2015.02.004>
- 1256 Fay, A. R., & McKinley, G. A. (2014). Global open-ocean biomes: Mean and temporal
 1257 variability. *Earth System Science Data*, 6(2), 273–284. <https://doi.org/10.5194/essd-6-273-2014>
- 1258 Fay, A. R., Gregor, L., Landschützer, P., McKinley, G. A., Gruber, N., Gehlen, M., ... & Zeng, J.
 1259 (2021). SeaFlux: harmonization of air–sea CO₂ fluxes from surface pCO₂ data products using a
 1260 standardized approach. *Earth System Science Data*, 13(10), 4693-4710.
 1261 <https://doi.org/10.5194/essd-13-4693-2021>
- 1262 Fernández-Castro, B., Álvarez, M., Nieto-Cid, M., Zunino, P., Mercier, H., & Álvarez-Salgado,
 1263 X. A. (2019). Dissolved organic nitrogen production and export by meridional overturning in the
 1264 eastern subpolar North Atlantic. *Geophysical Research Letters*, 46(7), 3832-3842.
 1265 <https://doi.org/10.1029/2018GL080284>
- 1266 Fontela, M., García-Ibáñez, M. I., Hansell, D. A., Mercier, H., & Pérez, F. F. (2016). Dissolved
 1267 organic carbon in the North Atlantic meridional overturning circulation. *Scientific reports*, 6(1),
 1268 26931. <https://doi.org/10.1038/srep26931>
- 1269 Fontela, M., Pérez, F. F., Mercier, H., & Lherminier, P. (2020). North Atlantic Western
 1270 Boundary Currents Are Intense Dissolved Organic Carbon Streams. *Frontiers in Marine Science*,
 1271 7, 593757. <https://doi.org/10.3389/fmars.2020.593757>
- 1272 Friedlingstein, P., Jones, M. W., O’Sullivan, M., Andrew, R. M., Bakker, D. C. E., Hauck, J., et
 1273 al. (2022). Global Carbon Budget 2021. *Earth System Science Data*, 14, 1917–2005.
 1274 <https://doi.org/10.5194/essd-14-1917-2022>
- 1275 Fröb, F., Olsen, A., Våge, K., Moore, K., Yashayaev, I., Jeansson, E., & Rajasakaren, B. (2016).
 1276 Irminger Sea deep convection injects oxygen and anthropogenic carbon to the ocean interior.
 1277 *Nature Communications*, 7, 13244. <https://doi.org/10.1038/ncomms13244>
- 1278 Fröb, F., Olsen, A., Becker, M., Chafik, L., Johannessen, T., Reverdin, G., & Omar, A. (2019).
 1279 Wintertime fCO₂ Variability in the Subpolar North Atlantic Since 2004. *Geophysical Research*
 1280 *Letter*, 46(3), 1580-1590. <https://doi.org/10.1029/2018gl080554>
- 1281 Gao, S., Schwinger, J., Tjiputra, J., Bethke, I., Hartmann, J., Mayorga, E., & Heinze, C. (2023).
 1282 Riverine impact on future projections of marine primary production and carbon uptake.
 1283 *Biogeosciences*, 20(1), 93-119. <https://doi.org/10.5194/bg-20-93-2023>
- 1284 Gerber, M., Joos, F., Vázquez-Rodríguez, M., Touratier, F., & Goyet, C. (2009). Regional air-sea
 1285 fluxes of anthropogenic carbon inferred with an Ensemble Kalman Filter. *Global biogeochemical*
 1286 *cycles*, 23(1). <https://doi.org/10.1029/2008GB003247>

- 1287 Gharamti, M., Tjiputra, J., Bethke, I., Samuelsen, A., Skjelvan, I., Bentsen, M., & Bertino, L.
1288 (2017). Ensemble data assimilation for ocean biogeochemical state and parameter estimation at
1289 different sites. *Ocean Modelling*, 112, 65-89. <https://doi.org/10.1016/j.ocemod.2017.02.006>
- 1290 Gehlen, M., Barciela, R., Bertino, L., Brasseur, P., Butenschön, M., Chai, F., et al. (2015).
1291 Building the capacity for forecasting marine biogeochemistry and ecosystems: recent advances
1292 and future developments, *Journal of Operational Oceanography*, 8, s168-s187.
1293 <https://doi.org/10.1080/1755876X.2015.1022350>
- 1294 Gloege, L., McKinley, G. A., Landschützer, P., Fay, A. R., Frölicher, T. L., Fyfe, J. C., et al.
1295 (2021). Quantifying errors in observationally based estimates of ocean carbon sink variability.
1296 *Global Biogeochemical Cycles*, 35(4), e2020GB006788. <https://doi.org/10.1029/2020GB006788>
- 1297 Goddijn-Murphy, L. M., Woolf, D. K., Land, P. E., Shutler, J. D., & Donlon, C. (2015). The
1298 OceanFlux Greenhouse Gases methodology for deriving a sea surface climatology of CO₂
1299 fugacity in support of air–sea gas flux studies. *Ocean Science*, 11(4), 519-541.
1300 <https://doi.org/10.5194/os-11-519-2015>
- 1301 González-Dávila, M., Santana-Casiano, J. M., Rueda, M. J., & Llinás, O. (2010). The water
1302 column distribution of carbonate system variables at the ESTOC site from 1995 to 2004.
1303 *Biogeosciences*, 7(10), 3067-3081. <https://doi.org/10.5194/bg-7-3067-2010>
- 1304 Gonzalez-Dávila, M., Santana Casiano, J. M., & Ucha, I. R. (2009). Seasonal variability of fCO₂
1305 in the Angola-Benguela region. *Progress in Oceanography*, 83, 124–133.
1306 <https://doi.org/10.1016/j.pocean.2009.07.033>
- 1307 Goris, N., Tjiputra, J. F., Olsen, A., Schwinger, J., Lauvset, S. K., and Jeansson, E. (2018)
1308 Constraining Projection-Based Estimates of the Future North Atlantic Carbon Uptake, *J.*
1309 *Climate*, 31, 3959–3978, <https://doi.org/10.1175/JCLI-D-17-0564.1>
- 1310 Goris, N., Johannsen, K., and Tjiputra, J. (2023). The emergence of the Gulf Stream and interior
1311 western boundary as key regions to constrain the future North Atlantic carbon uptake. *Geosci.*
1312 *Model Dev.*, 16, 2095–2117, <https://doi.org/10.5194/gmd-16-2095-2023>.
- 1313 Gregor, L., Lebehot, A. D., Kok, S., & Scheel Monteiro, P. M. (2019). A comparative
1314 assessment of the uncertainties of global surface ocean CO₂ estimates using a machine-learning
1315 ensemble (CSIR-ML6 version 2019a)–have we hit the wall?. *Geoscientific Model Development*,
1316 12(12), 5113-5136. <https://doi.org/10.5194/gmd-12-5113-2019>
- 1317 Gregor, L., & Gruber, N. (2021). OceanSODA-ETHZ: a global gridded data set of the surface
1318 ocean carbonate system for seasonal to decadal studies of ocean acidification. *Earth System*
1319 *Science Data*, 13(2), 777-808. <https://doi.org/10.5194/essd-13-777-2021>
- 1320 Gruber, N., Keeling, C. D., & Stocker, T. F. (1998). Carbon-13 constraints on the seasonal
1321 inorganic carbon budget at the BATS site in the northwestern Sargasso Sea. *Deep Sea Research*
1322 *Part I: Oceanographic Research Papers*, 45(4-5), 673-717. [https://doi.org/10.1016/S0967-0637\(97\)00098-8](https://doi.org/10.1016/S0967-0637(97)00098-8)
- 1324 Gruber, N., Keeling, C. D., & Bates, N. R. (2002). Interannual variability in the North Atlantic
1325 Ocean carbon sink. *Science*, 298(5602), 2374-2378. <https://doi.org/10.1126/science.1077077>
- 1326 Gruber, N., Clement, D., Carter, B. R., Feely, R. A., van Heuven, S., Hoppema, M., et al. (2019).
1327 The oceanic sink for anthropogenic CO₂ from 1994 to 2007. *Science*, 363(6432), 1193–1199.

- 1328 <https://doi.org/10.1126/science.aau5153>
- 1329 Gruber, N., Gloor, M., Mikaloff Fletcher, S. E., Doney, S. C., Dutkiewicz, S., Follows, M., et al.
1330 (2009). Oceanic sources, sinks, and transport of atmospheric CO₂, *Global Biogeochemical*
1331 *Cycles*, 23, GB1005. <https://doi.org/10.1029/2008GB003349>
- 1332 Haine, T. W. N. (2016), Vagaries of Atlantic overturning, *Nat. Geosci.*, 9, 479– 480.
1333 <https://www.nature.com/articles/ngeo2748>
- 1334 Hansell, D. A. (2013). Recalcitrant dissolved organic carbon fractions. *Annual review of marine*
1335 *science*, 5, 421-445. [https://www.annualreviews.org/doi/abs/10.1146/annurev-marine-120710-](https://www.annualreviews.org/doi/abs/10.1146/annurev-marine-120710-100757)
1336 [100757](https://www.annualreviews.org/doi/abs/10.1146/annurev-marine-120710-100757)
- 1337 Hassoun, A. E. R., Gemayel, E., Krasakopoulou, E., Goyet, C., Saab, M. A.-A., Guglielmi, V., et
1338 al. (2015). Acidification of the Mediterranean Sea from anthropogenic carbon penetration. *Deep*
1339 *Sea Res. Pt. I Oceanogr Res Pap* 102:115. <http://doi.org/10.1016/j.dsr.2015.04.005>.
- 1340 Hauck, J. and Völker, C. (2015). Rising atmospheric CO₂ leads to large impact of biology on
1341 Southern Ocean CO₂ uptake via changes of the Revelle factor. *Geophys. Res. Lett.*, 42: 1459–
1342 1464. doi: [10.1002/2015GL063070](https://doi.org/10.1002/2015GL063070).
- 1343 Hauck, J., Zeising, M., Le Quéré, C., Gruber, N., Bakker, D. C. E., Bopp, L., et al. (2020).
1344 Consistency and Challenges in the Ocean Carbon Sink Estimate for the Global Carbon Budget.
1345 *Frontiers in Marine Science*, 7(October), 1–22. <https://doi.org/10.3389/fmars.2020.571720>
- 1346 Hauck, J., Nissen, C., Landschützer, P., Rödenbeck, C., Bushinsky, S. & Olsen, A. (2023).
1347 Sparse observations induce large biases in estimates of the global ocean CO₂ sink: an ocean
1348 model subsampling experiment. *Phil. Trans. R. Soc. A.*, 381, 20220063.
1349 <http://doi.org/10.1098/rsta.2022.0063>
- 1350 Hauck, J., Gregor, L., Nissen, C., Patara, L., Hague, M., Mongwe, N. P., et al. (submitted). The
1351 Southern Ocean carbon cycle 1985-2018: mean, seasonal cycle, trends and storage. *Global*
1352 *Biogeochemical Cycles*. Submitted
- 1353 Hirschi, J. J.-M., Barnier, B., Böning, C., Biastoch, A., Blaker, A. T., Coward, A., et al. (2020).
1354 The Atlantic meridional overturning circulation in high-resolution models. *Journal of*
1355 *Geophysical Research: Oceans*, 125, e2019JC015522. <https://doi.org/10.1029/2019JC015522>
- 1356 Ho, D. T., Law, C. S., Smith, M. J., Schlosser, P., Harvey, M., & Hill, P. (2006). Measurements
1357 of air-sea gas exchange at high wind speeds in the Southern Ocean: Implications for global
1358 parameterizations. *Geophysical Research Letters*, 33(16).
1359 <https://doi.org/10.1029/2006GL026817>
- 1360 Holfort, J., Johnson, K. M., Schneider, B., Siedler, G., & Wallace, D. W. (1998). Meridional
1361 transport of dissolved inorganic carbon in the South Atlantic Ocean. *Global Biogeochemical*
1362 *Cycles*, 12(3), 479-499. <https://doi.org/10.1029/98GB01533>
- 1363 Huertas, I. E., Ríos, A. F., García-Lafuente, J., Makaoui, A., Rodríguez-Gálvez, S., Sánchez-
1364 Román, A., ... & Pérez, F. F. (2009). Anthropogenic and natural CO₂ exchange through the
1365 Strait of Gibraltar. *Biogeosciences*, 6(4), 647-662. <https://doi.org/10.5194/bg-6-647-2009>
- 1366 Iida, Y., Takatani, Y., Kojima, A., & Ishii, M. (2021). Global trends of ocean CO₂ sink and
1367 ocean acidification: an observation-based reconstruction of surface ocean inorganic carbon
1368 variables. *Journal of Oceanography*, 77, 323-358. <https://doi.org/10.1007/s10872-020-00571-5>

- 1369 Ibánhez, J. S. P., Araujo, M., & Lefèvre, N. (2016). The overlooked tropical oceanic CO₂ sink.
1370 *Geophysical Research Letter*, 43, 3804–3812. <https://doi.org/10.1002/2016GL068020>
- 1371 Ingrosso, G., Giani, M., Comici, C., Kralj, M., Piacentino, S., De Vittor, C., et al. (2016) Drivers
1372 of the carbonate system seasonal variations in a Mediterranean gulf. *Estuar. Coast. Shelf Sci.*
1373 168: 58–70. <http://doi.org/10.1016/j.ecss.2015.11.001>
- 1374 Ito, R. G., Schneider, B., & Thomas, H. (2005). Distribution of surface fCO₂ and air-sea fluxes in
1375 the Southwestern subtropical Atlantic and adjacent continental shelf. *Journal of Marine Systems.*
1376 56, 227– 242. <https://doi.org/10.1016/j.jmarsys.2005.02.005>
- 1377 Jacobson, A. R., Mikaloff Fletcher, S. E., Gruber, N., Sarmiento, J. L., & Gloor, M. (2007). A
1378 joint atmosphere-ocean inversion for surface fluxes of carbon dioxide: 2. Regional results.
1379 *Global Biogeochemical Cycles*, 21(1) <https://doi.org/10.1029/2006GB002703>
- 1380 Jeansson, E., Olsen, A., Eldevik, T., Skjelvan, I., Omar, A. M., Lauvset, S. K., et al. (2011). The
1381 Nordic Seascarbon budget: Sources, sinks, and uncertainties. *Global Biogeochemical Cycles*,
1382 25(4), GB4010. <https://doi.org/10.1029/2010GB003961>
- 1383 Jing, Y., Li, Y., Xu, Y. & Fan, G. (2019). Influences of the NAO on the North Atlantic CO₂
1384 Fluxes in Winter and Summer on the Interannual Scale. *Adv. Atmos. Sci.* 36, 1288–1298.
1385 <https://doi.org/10.1007/s00376-019-8247-2>
- 1386 Kapsenberg, L., Alliouane, S., Gazeau, F., Mousseau, L., & Gattuso, J.-P. (2017). Coastal ocean
1387 acidification and increasing total alkalinity in the northwestern Mediterranean Sea. *Ocean*
1388 *Science* 13, 411–426. <https://doi.org/10.5194/os-13-411-2017>
- 1389 Keeling, C. D. (1993). Lecture 2: Surface ocean CO₂. In *The global carbon cycle* (pp. 413-429).
1390 Springer Berlin Heidelberg. https://doi.org/10.1007/978-3-642-84608-3_17
- 1391 Keeling, R. F. & Peng, T-H. (1995). Transport of heat, CO₂ and O₂ by the Atlantic's
1392 thermohaline circulation. *Philosophical Transactions of the Royal Society of London B*, 348,
1393 133-142. <https://doi.org/10.1098/rstb.1995.0055>
- 1394 Khatiwala, S., Primeau, F., & Hall, T. (2009). Reconstruction of the history of anthropogenic
1395 CO₂ concentrations in the ocean. *Nature*, 462(7271), 346-
1396 349. <https://doi.org/10.1038/nature08526>
- 1397 Khatiwala, S., Tanhua, T., Mikaloff Fletcher, S., Gerber, M., Doney, S. C., Graven, H. D., ... &
1398 Sabine, C. L. (2013). Global ocean storage of anthropogenic carbon. *Biogeosciences*, 10(4),
1399 2169-2191. <https://doi.org/10.5194/bg-10-2169-2013>
- 1400 Körtzinger, A. (2003). A significant CO₂ sink in the tropical Atlantic Ocean associated with the
1401 Amazon River plume. *Geophysical Research Letter*, 30(24), 2287.
1402 <https://doi.org/10.1029/2003GL018841>
- 1403 Krasakopoulou E., Rapsomanikis, S., Papadopoulos, A., Papathanassiou, E. (2009) Partial
1404 pressure and air-sea CO₂ flux in the Aegean Sea during February 2006. *Cont Shelf Res*, 29:
1405 1477-1488. <https://doi.org/10.1016/j.csr.2009.03.015>
- 1406 Krasakopoulou, E., Souvermezoglou, E., Goyet, C. (2017). Carbonate system parameters and
1407 anthropogenic CO₂ in the North Aegean Sea during October 2013. *Cont Shelf Res* 149: 69-81.
1408 <https://doi.org/10.1016/j.csr.2017.04.002>

- 1409 Lacroix, F., Ilyina, T., & Hartmann, J. (2020). Oceanic CO₂ outgassing and biological
1410 production hotspots induced by pre-industrial river loads of nutrients and carbon in a global
1411 modeling approach. *Biogeosciences*, 17(1), 55-88. <https://doi.org/10.5194/bg-17-55-2020>
- 1412 Landschützer, P., Gruber, N., E. Bakker, D. C., & Schuster, U. (2014), Recent variability of the
1413 global ocean carbon sink, *Global Biogeochemical Cycles*, 28, 927– 949.
1414 <https://doi.org/10.1002/2014GB004853>
- 1415 Lefèvre, N., Diverrès, D., & Gallois, F. (2010). Origin of CO₂ undersaturation in the western
1416 tropical Atlantic, *Tellus B*, 62(5), 595–607, <https://doi.org/10.1111/j.1600-0889.2010.00475.x>
- 1417 Leseurre, C., Lo Monaco, C., Reverdin, G., Metzl, N., Fin, J., Olafsdottir, S., & Racapé, V.
1418 (2020). Ocean carbonate system variability in the North Atlantic Subpolar surface water (1993–
1419 2017). *Biogeosciences*, 17(9), 2553-2577. <https://doi.org/10.5194/bg-17-2553-2020>
- 1420 Le Quéré, C., Andrew, R. M., Friedlingstein, P., Sitch, S., Hauck, J., Pongratz, J., et al. (2018),
1421 Global Carbon Budget. *Earth Syst. Sci. Data*, 10, 2141–2194. [https://doi.org/10.5194/essd-10-](https://doi.org/10.5194/essd-10-2141-2018)
1422 [2141-2018](https://doi.org/10.5194/essd-10-2141-2018)
- 1423 Louchard, D., Gruber, N., & Münnich, M. (2021). The Impact of the Amazon on the Biological
1424 Pump and the Air-Sea CO₂ Balance of the Western Tropical Atlantic. *Global Biogeochemical*
1425 *Cycles*, 35(6). <https://doi.org/10.1029/2020GB006818>
- 1426 Ma, X., Jing, Z., Chang, P., Liu, X., Montuoro, R., Small, R. J., ... & Wu, L. (2016). Western
1427 boundary currents regulated by interaction between ocean eddies and the atmosphere. *Nature*,
1428 535(7613), 533-537. <https://doi.org/10.1038/nature18640>
- 1429 Macdonald, A. M., Baringer, M. O., Wanninkhof, R., Lee, K. & Wallace, D. W. R. (2003). A
1430 1998_1992 comparison of inorganic carbon and its transport across 24.5°N in the Atlantic. *Deep-*
1431 *Sea Research. II*, 50, 3041-3064 (2003). <https://doi.org/10.1016/j.dsr2.2003.07.009>
- 1432 Macovei, V. A., Hartman, S. E., Schuster, U., Torres-Valdés, S., Moore, C. M., & Sanders, R. J.
1433 (2020). Impact of physical and biological processes on temporal variations of the ocean carbon
1434 sink in the mid-latitude North Atlantic (2002–2016). *Progress in Oceanography*, 180, 102223
1435 [.https://doi.org/10.1016/j.pocean.2019.102223](https://doi.org/10.1016/j.pocean.2019.102223)
- 1436 McKinley, G. A., Fay, A. R., Eddebar, Y. A., Gloege, L., & Lovenduski, N. S. (2020). External
1437 forcing explains recent decadal variability of the ocean carbon sink. *Agua Advances*, 1(2),
1438 e2019AV000149. <https://doi.org/10.1029/2019AV000149>
- 1439 McKinley, G. A., Ritzer, A. L., & Lovenduski, N. S. (2018). Mechanisms of northern North
1440 Atlantic biomass variability. *Biogeosciences*, 15, 6049–6066, [https://doi.org/10.5194/bg-15-](https://doi.org/10.5194/bg-15-6049-2018)
1441 [6049-2018](https://doi.org/10.5194/bg-15-6049-2018)
- 1442 Michaels, A. F., Bates, N. R., Buesseler, K. O., Carlson, C. A., & Knap, A. H. (1994). Carbon-
1443 cycle imbalances in the Sargasso Sea. *Nature*, 372(6506), 537-540.
1444 <https://doi.org/10.1038/372537a0>
- 1445 Mikaloff Fletcher, S. E., Gruber, N., Jacobson, A. R., Doney, S. C., Dutkiewicz, S., Gerber, M.,
1446 et al. (2006). Inverse estimates of anthropogenic CO₂ uptake, transport, and storage by the
1447 ocean. *Global Biogeochemical Cycles*, 20(2), GB2002. <https://doi.org/10.1029/2005GB002530>
- 1448 Mikaloff-Fletcher, S. E. , Gruber, N., Jacobson, A. R., Gloor, M., Doney, S. C., Dutkiewicz, S.,
1449 et al. (2007). Inverse estimates of the oceanic sources and sinks of natural CO₂ and the implied

- 1450 oceanic carbon transport. *Global Biogeochemical Cycles*. 21, GB1010 (2007).
1451 <https://doi.org/10.1029/2006GB002751>
- 1452 Olsen, A., Key, R. M., Van Heuven, S., Lauvset, S. K., Velo, A., Lin, X., ... & Suzuki, T. (2016).
1453 The Global Ocean Data Analysis Project version 2 (GLODAPv2)—an internally consistent data
1454 product for the world ocean. *Earth System Science Data*, 8(2), 297-
1455 323. <https://doi.org/10.5194/essd-8-297-2016>
- 1456 Olsen, A., Brown, K. R., Chierici, M., Johannessen, T., & Neill, C. (2008). Sea-surface CO₂
1457 fugacity in the subpolar North Atlantic. *Biogeosciences*, 5(2), 535-547.
1458 <https://doi.org/10.5194/bg-5-535-2008>
- 1459 Olsen, A., Lange, N., Key, R. M., Tanhua, T., Álvarez, M., Becker, S., ... & Wanninkhof, R.
1460 (2019). GLODAPv2. 2019—an update of GLODAPv2. *Earth System Science Data*, 11(3), 1437-
1461 1461. <https://doi.org/10.5194/essd-11-1437-2019>
- 1462 Padin, X. A., Vazquez-Rodriguez, M., Castaño, M., Velo, A., Alonso-Perez, F., Gago, J., et al.
1463 (2010). Air-Sea CO₂ fluxes in the Atlantic as measured during boreal spring and autumn.
1464 *Biogeosciences*, 7, 1587–1606. <https://doi.org/10.5194/bg-7-1587-2010>
- 1465 Park, G. -H., Wanninkhof, R., Doney, S. C., Takahashi, T., Lee, K., Feely, R. A., et al. (2010).
1466 Variability of global net sea–air CO₂ fluxes over the last three decades using empirical
1467 relationships. *Tellus B*, 62, 352-368. <https://doi.org/10.1111/j.1600-0889.2010.00498.x>
- 1468 Petihakis, G., Perivoliotis, L., Korres, G., Ballas, D., Frangoulis, C., Pagonis, P., ... & Zisis, N.
1469 (2018). An integrated open-coastal biogeochemistry, ecosystem and biodiversity observatory of
1470 the eastern Mediterranean—the Cretan Sea component of the POSEIDON system. *Ocean Science*,
1471 14(5), 1223-1245. <https://doi.org/10.5194/os-14-1223-2018>
- 1472 Pérez, F. F., Vázquez-Rodríguez, M., Louarn, E., Padín, X. A., Mercier, H., & Ríos, A. F.
1473 (2008). Temporal variability of the anthropogenic CO₂ storage in the Irminger Sea.
1474 *Biogeosciences*, 5(6), 1669-1679. <https://doi.org/10.5194/bg-5-1669-2008>
- 1475 Pérez, F. F., Mercier, H., Vázquez-Rodríguez, M., Lherminier, P., Velo, A., Pardo, P. C., et al.
1476 (2013). Atlantic Ocean CO₂ uptake reduced by weakening of the meridional overturning
1477 circulation. *Nature Geoscience*, 6(2), 146–152. <https://doi.org/10.1038/ngeo1680>
- 1478 Pfeil B., Olsen, A., Bakker, D. C. E., Hankin, S., Koyuk, H., Kozyr, A., et al. (2013). A uniform,
1479 quality controlled surface ocean CO₂ atlas (SOCAT). *Earth System Science Data*, 5, 125–143.
1480 <https://doi.org/10.5194/essd-5-125-2013>
- 1481 Racapé, V., Zunino, P., Mercier, H., Lherminier, P., Bopp, L., Pérez, F. F., & Gehlen, M. (2018).
1482 Transport and storage of anthropogenic C in the North Atlantic Subpolar Ocean. *Biogeosciences*,
1483 15(14), 4661–4682. <https://doi.org/10.5194/bg-15-4661-2018>
- 1484 Regnier, P., Resplandy, L., Najjar, R. G., & Ciais, P. (2022). The land-to-ocean loops of the
1485 global carbon cycle. *Nature*, 603(7901), 401-410. <https://doi.org/10.1038/s41586-021-04339-9>
- 1486 Regnier, P., Friedlingstein, P., Ciais, P., Mackenzie, F. T., Gruber, N., Janssens, I. a., et al.
1487 (2013). Anthropogenic perturbation of the carbon fluxes from land to ocean. *Nature Geoscience*,
1488 6(8), 597–607. <https://doi.org/10.1038/ngeo1830>
- 1489 Resplandy, L., Keeling, R. F., Rödenbeck, C., Stephens, B. B., Khatiwala, S., Rodgers, K. B., et
1490 al.(2018). Revision of global carbon fluxes based on a reassessment of oceanic and riverine

- 1491 carbon transport. *Nature Geoscience*, 11, 504–509. <https://doi.org/10.1038/s41561-018-0151-3>
- 1492 Rhein, M., D. Kieke, and R. Steinfeldt (2015), Advection of North Atlantic Deep Water from the
1493 Labrador Sea to the southern hemisphere, *J. Geophys. Res. Oceans*, 120, 2471–2487,
1494 <https://doi.org/10.1002/2014JC010605>
- 1495 Rhein, M., Steinfeldt, R., Kieke, D., Stendardo, I., & Yashayaev, I. (2017). Ventilation
1496 variability of Labrador Sea Water and its impact on oxygen and anthropogenic carbon: a review.
1497 *Philosophical Transactions A*, 375, 20160321. <http://dx.doi.org/10.1098/rsta.2016.0321>
- 1498 Ríos, A. F., Álvarez-Salgado, X. A., Pérez, F. F., Bingler, L. S., Arístegui, J., & Mémery, L.
1499 (2003). Carbon dioxide along WOCE line A14: Water masses characterization and
1500 anthropogenic entry. *Journal of Geophysical Research: Oceans*, 108(C4).
1501 <https://doi.org/10.1029/2000JC000366>
- 1502 Ríos, A. F., Velo, A., Pardo, P. C., Hoppema, M., & Pérez, F. F. (2012). An update of
1503 anthropogenic CO₂ storage rates in the western South Atlantic basin and the role of Antarctic
1504 Bottom Water. *Journal of Marine Systems*, 94, 197-
1505 203. <https://doi.org/10.1016/j.jmarsys.2011.11.023>
- 1506 Rödenbeck et al., 2014, Rödenbeck, C., Bakker, D. C. E., Metzl, N., Olsen, A., Sabine, C.,
1507 Cassar, N., Reum, F., Keeling, R. F., and Heimann, M. (2014) Interannual sea–air CO₂ flux
1508 variability from an observation driven ocean mixed-layer scheme, *Biogeosciences*, 11, 4599–
1509 4613, <https://doi.org/10.5194/bg-11-4599-2014>
- 1510 Rödenbeck, C., Bakker, D. C. E., Gruber, N., Iida, Y., Jacobson, A. R., Jones, S., et al. (2015).
1511 Data-based estimates of the ocean carbon sink variability – first results of the Surface Ocean
1512 pCO₂ Mapping intercomparison (SOCOM), *Biogeosciences*, 12, 7251– 7278,
1513 <https://doi.org/10.5194/bg-12-7251-2015>
- 1514 Rödenbeck, C., DeVries, T., Hauck, J., Le Quéré, C., & Keeling, R. F. (2022). Data-based
1515 estimates of interannual sea–air CO₂ flux variations 1957–2020 and their relation to
1516 environmental drivers. *Biogeosciences*, 19, 2627–2652, <https://doi.org/10.5194/bg-19-2627-2022>
- 1517 Rödenbeck, C., Keeling, R. F., Bakker, D. C. E., Metzl, N., Olsen, A., Sabine, C., & Heimann, M.
1518 (2013). Global surface-ocean pCO₂ and sea–air CO₂ flux variability from an observation-driven
1519 ocean mixed-layer scheme, *Ocean Sciences*, 9, 193–216. <https://doi.org/10.5194/os-9-193-2013>
- 1520 Rodgers, K. B., Schwinger, J., Fassbender, A. J., Landschützer, P., Yamaguchi, R., Frenzel, H.,
1521 et al. (in review). Seasonal variability of the surface ocean carbon cycle: a synthesis. *Global*
1522 *Biogeochemical Cycles*.
- 1523 Roshan, S., & DeVries, T. (2017). Efficient dissolved organic carbon production and export in
1524 the oligotrophic ocean. *Nature communications*, 8(1), 2036. <https://doi.org/10.1038/s41467-017-02227-3>
- 1526 Rosón, G. (2003). Carbon distribution, fluxes, and budgets in the subtropical North Atlantic
1527 Ocean (24.5°N). *Journal of Geophysical Research*, 108(C5), 3144.
1528 <https://doi.org/10.1029/1999JC000047>
- 1529 Sabine, C. L., Hankin, S., Koyuk, H., Bakker, D. C. E., Pfeil, B., Olsen, A., et al. (2013). Surface
1530 ocean CO₂ Atlas (SOCAT) gridded data products. *Earth System Science.Data*, 5, 145–153.
1531 <https://doi.org/10.5194/essd-5-145-2013>

- 1532 Sabine, C. L., Feely, R. A., Gruber, N., Key, R. M., Lee, K., Bullister, J. L., et al. (2004). The
 1533 Oceanic Sink for Anthropogenic CO₂, *Science*, 305, 367–371, 2004.
 1534 <https://doi.org/10.1126/science.1097403>
- 1535 Santana-Casiano, J. M., González-Dávila, M., Rueda, M., Llinás, O., and González-Dávila, E.-
 1536 F.(2007).: The interannual variability of oceanic CO₂ parameters in the northeast Atlantic
 1537 subtropical gyre at the ESTOC site, *Global Biogeochem. Cy.*, 21, GB1015,
 1538 <https://doi.org/10.1029/2006GB002788>
- 1539 Santana-Casiano, J. M., González-Dávila, M., & Ucha, I. R. (2009). Carbon dioxide fluxes in the
 1540 Benguela upwelling system during winter and spring: A comparison between 2005 and 2006.
 1541 *Deep Sea Research Part II: Topical Studies in Oceanography*, 56(8-10), 533-541.
 1542 <https://doi.org/10.1016/j.dsr2.2008.12.010>
- 1543 Schneider, A., Tanhua, T., Körtzinger, A., & Wallace, D. W. (2010). High anthropogenic carbon
 1544 content in the eastern Mediterranean. *Journal of Geophysical Research: Oceans*, 115(C12).
 1545 <https://doi.org/10.1029/2010JC006171>
- 1546 Schuster, U., McKinley, G. A., Bates, N., Chevallier, F., Doney, S. C., Fay, A. R., et al. (2013).
 1547 An assessment of the Atlantic and Arctic sea–air CO₂ fluxes, 1990–2009. *Biogeosciences*, 10,
 1548 607–627, <https://doi.org/10.5194/bg-10-607-2013>
- 1549 Schwinger, J., Goris, N., Tjiputra, J. F., Kriest, I., Bentsen, M., Bethke, I., et al. (2016).
 1550 Evaluation of NorESM-OC (versions 1 and 1.2), the ocean carbon-cycle stand-alone
 1551 configuration of the Norwegian Earth System Model (NorESM1). *Geoscientific Model
 1552 Development*, 9(8), 2589-2622. <https://doi.org/10.5194/gmd-9-2589-2016>
- 1553 Séférian, R., Gehlen, M., Bopp, L., Resplandy, L., Orr, J. C., Marti, O., et al. (2016). Inconsistent
 1554 strategies to spin up models in CMIP5: implications for ocean biogeochemical model
 1555 performance assessment, *Geoscientific Model Development*, 9, 1827–1851.
 1556 <https://doi.org/10.5194/gmd-9-1827-2016>
- 1557 Séférian, R., Berthet, S., Yool, A., Palmieri, J., Bopp, L., Tagliabue, A., et al. (2020). Tracking
 1558 Improvement in Simulated Marine Biogeochemistry Between CMIP5 and CMIP6. *Current
 1559 Climate Change Reports*, 6, 95–119. <https://doi.org/10.1007/s40641-020-00160-0>
- 1560 Sisma-Ventura, G., Or, B. M., Yam, R., Herut, B., & Silverman, J. (2017) pCO₂ variability in the
 1561 surface waters of the ultra-oligotrophic Levantine Sea: exploring the air-sea CO₂ fluxes in a fast
 1562 warming region. *Mar. Chem.* 196: 13–23. <https://doi.org/10.1016/j.marchem.2017.06.006>
- 1563 Steinfeldt, R., Rhein, M., Bullister, J. L., & Tanhua, T. (2009). et al. 2009 GBC Inventory
 1564 changes in anthropogenic carbon from 1997–2003 in the Atlantic Ocean between 20°S and
 1565 65°N. *Global Biogeochemical Cycles*, 23, GB3010.
 1566 <https://doi.org/10.1029/2008GB003311>
- 1567 Stöven T. and T. Tanhua, (2014) Ventilation of the Mediterranean Sea constrained by multiple
 1568 transient tracer measurements. *Ocean Sci.*, 10, 439–457, <https://doi.org/10.5194/os-10-439-2014>
- 1569 Sarmiento, J. L., & Sundquist, E. T. (1992). Revised budget for the oceanic uptake of
 1570 anthropogenic carbon dioxide. *Nature*, 356(6370), 589-593. <https://doi.org/10.1038/356589a0>
- 1571 Takahashi, T. (1961). Carbon dioxide in the atmosphere and Atlantic Ocean water. *Journal of
 1572 Geophysical. Research.*, 66, 477-494. <https://doi.org/10.1029/JZ066i002p00477>

- 1573 Takahashi, T., Olafsson, J., Goddard, J., Chipman, D. & Sutherland, S. (1993). Seasonal
1574 variation of CO₂ and nutrients in the high-latitude surface oceans: a comparative study. *Global*
1575 *Biogeochemical Cycles*, 7, 843–878. <https://doi.org/10.1029/93GB02263>
- 1576 Takahashi, T., Sutherland, S. C., Sweeney, C., Poisson, A., Metzl, N., Tillbrook, B., et al.
1577 (2002). Global sea-air CO₂ flux based on climatological surface ocean pCO₂, and seasonal
1578 biological and temperature effects. *Deep-Sea Research II*, 49, 1601-1622,
1579 [https://doi.org/10.1016/S0967-0645\(02\)00003-6](https://doi.org/10.1016/S0967-0645(02)00003-6)
- 1580 Takahashi, T., Sutherland, S. C., Wanninkhof, R., Sweeney, C., Feely, R. A., Chipman, D. W.,
1581 et al. (2009). Climatological mean and decadal change in surface ocean pCO₂ and net sea-air
1582 CO₂ flux over the global oceans. *Deep-Sea Research II*, 56, 554-577,
1583 <https://doi.org/10.1016/j.dsr2.2008.12.009>
- 1584 Terhaar, J., Frölicher, T. L., & Joos, F. (2022). Observation-constrained estimates of the global
1585 ocean carbon sink from Earth system models. *Biogeosciences*, 19, 4431–4457.
1586 <https://doi.org/10.5194/bg-19-4431-2022>
- 1587 Terhaar, J., Goris, N., Müller, J.D., DeVries, T., Gruber, N., Hauck, J., Perez, F. & Séférian, R.
1588 (submitted). Assessment of Global Ocean Biogeochemistry Models for Ocean Carbon Sink
1589 Estimates in RECCAP2 and Recommendations for Future Studies. *Global Biogeochemical*
1590 *Cycles*.
- 1591 Thomas, H., Friederike Prowe, A. E., Lima, I. D., Doney, S. C., Wanninkhof, R., Greatbatch, R.
1592 J., et al. (2008). Changes in the North Atlantic Oscillation influence CO₂ uptake in the North
1593 Atlantic over the past 2 decades. *Global Biogeochemical Cycles*, 22, GB4027,
1594 <https://doi.org/10.1029/2007GB003167>
- 1595 Tjiputra, J. F., Polzin, D., & Winguth, A. M. (2007). Assimilation of seasonal chlorophyll and
1596 nutrient data into an adjoint three-dimensional ocean carbon cycle model: Sensitivity analysis
1597 and ecosystem parameter optimization. *Global biogeochemical cycles*,
1598 *21*(1). <https://doi.org/10.1029/2006GB002745>
- 1599 Tjiputra, J. F., Assmann, K., & Heinze, C. (2010). Anthropogenic carbon dynamics in the
1600 changing ocean, *Ocean Sciences*, 6, 605–614. <https://doi.org/10.5194/os-6-605-2010>
- 1601 Tjiputra, J. F., Olsen, A., Assmann, K., Pfeil, B., & Heinze, C. (2012). A model study of the
1602 seasonal and long-term North Atlantic surface pCO₂ variability. *Biogeosciences*, 9, 907–923,
1603 <https://doi.org/10.5194/bg-9-907-2012>
- 1604 Tjiputra, J. F., Olsen, A. R. E., Bopp, L., Lenton, A., Pfeil, B., Roy, T., ... & Heinze, C. (2014).
1605 Long-term surface pCO₂ trends from observations and models. *Tellus B: Chemical and Physical*
1606 *Meteorology*, 66(1), 23083. <https://doi.org/10.3402/tellusb.v66.23083>
- 1607 Touratier, F., Goyet, C., Houpert, L., de Madron, X. D., Lefèvre, D., Stabholz, M., & Guglielmi,
1608 V. (2016). Role of deep convection on anthropogenic CO₂ sequestration in the Gulf of Lions
1609 (northwestern Mediterranean Sea). *Deep Sea Research Part I*, 113, 33–48.
1610 <https://doi.org/10.1016/j.dsr.2016.04.003>
- 1611 Ullman, D. J., McKinley, G. A., Bennington, V., & Dutkiewicz, S. (2009). Trends in the North
1612 Atlantic carbon sink: 1992–2006. *Global Biogeochemical Cycles*, 23(4).
1613 <https://doi.org/10.1029/2008GB003383>

- 1614 Urbini, L., Ingrosso, G., Djakovac, T., Piacentino, S. & Giani, M. (2020) Temporal and Spatial
 1615 Variability of the CO₂ System in a Riverine Influenced Area of the Mediterranean Sea, the
 1616 Northern Adriatic. *Front. Mar. Sci.* 7:679. <https://doi.org/10.3389/fmars.2020.00679>
- 1617 Vaittinada Ayar, P., Bopp, L., Christian, J. R., Ilyina, T., Krasting, J. P., Séférian, R., et al.
 1618 (2022). Contrasting projections of the ENSO-driven CO₂ flux variability in the equatorial Pacific
 1619 under high-warming scenario, *Earth System Dynamics*, 13, 1097–1118.
 1620 <https://doi.org/10.5194/esd-13-1097-2022>
- 1621 Wanninkhof, R. (1992). Relationship between wind speed and gas exchange over the ocean.
 1622 *Journal of Geophysical Research: Oceans*, 97(C5), 7373-7382.
 1623 <https://doi.org/10.1029/92JC00188>
- 1624 Wanninkhof, R., Park, G. H., Takahashi, T., Sweeney, C., Feely, R., Nojiri, Y., et al. (2013).
 1625 Global ocean carbon uptake: Magnitude, variability and trends. *Biogeosciences*, 10, 1983–2000.
 1626 <https://doi.org/10.5194/bg-10-1983-2013>
- 1627 Wanninkhof, R. (2014). Relationship between wind speed and gas exchange over the ocean
 1628 revisited. *Limnology and Oceanography: Methods*, 12(6), 351-
 1629 362. <https://doi.org/10.4319/lom.2014.12.351>
- 1630 Wanninkhof, R., Pickers, P. A., Omar, A. M., Sutton, A., Murata, A., Olsen, A., et al. (2019). A
 1631 Surface Ocean CO₂ Reference Network, SOCONET and Associated Marine Boundary Layer
 1632 CO₂ Measurements. *Frontiers in Marine Science*, 6:400.
 1633 <https://doi.org/10.3389/fmars.2019.00400>
- 1634 Watson, A. J., Nightingale, P. D., & Cooper, D. J. (1995). Modelling atmosphere—ocean CO₂
 1635 transfer. *Philosophical Transactions of the Royal Society of London. Series B: Biological*
 1636 *Sciences*, 348(1324), 125-132. <https://doi.org/10.1098/rstb.1995.0054>
- 1637 Watson, A. J., Schuster, U., Bakker, D. C., Bates, N. R., Corbière, A., González-Dávila, M., ... &
 1638 Wanninkhof, R. (2009). Tracking the variable North Atlantic sink for atmospheric CO₂. *Science*,
 1639 326(5958), 1391-1393. <https://doi.org/10.1126/science.1177394>
- 1640 Watson, A. J., Schuster, U., Shutler, J. D., Holding, T., Ashton, I. G., Landschützer, P., ... &
 1641 Goddijn-Murphy, L. (2020). Revised estimates of ocean-atmosphere CO₂ flux are consistent
 1642 with ocean carbon inventory. *Nature communications*, 11(1), 4422.
 1643 <https://doi.org/10.1038/s41467-020-18203-3>
- 1644 Wilkin, J. L., Mansbridge, J. V., & Godfrey, J. S. (1995). Pacific Ocean heat transport at 24 N in
 1645 a high-resolution global model. *Journal of physical oceanography*, 25(10), 2204-2214.
 1646 [https://doi.org/10.1175/1520-0485\(1995\)025%3C2204:POHTAI%3E2.0.CO;2](https://doi.org/10.1175/1520-0485(1995)025%3C2204:POHTAI%3E2.0.CO;2)
- 1647 Wimart-Rousseau, C., Wagener, T., Álvarez, M., Moutin, T., Fourrier, M., Coppola, L., ... &
 1648 Lefèvre, D. (2021). Seasonal and interannual variability of the CO₂ system in the Eastern
 1649 Mediterranean Sea: A case study in the north Western levantine basin. *Frontiers in Marine*
 1650 *Science*, 8, 649246. <https://doi.org/10.3389/fmars.2021.649246>
- 1651 Wallace, D. W. (2001). Storage and transport of excess CO₂ in the oceans: The JGOFS/WOCE
 1652 global CO₂ survey. In *International Geophysics* (Vol. 77, pp. 489-L). Academic Press.
 1653 [https://doi.org/10.1016/S0074-6142\(01\)80136-4](https://doi.org/10.1016/S0074-6142(01)80136-4)
- 1654 Woolf, D. K., Land, P. E., Shutler, J. D., Goddijn-Murphy, L. M., & Donlon, C. J. (2016). On the

- 1655 calculation of air-sea fluxes of CO₂ in the presence of temperature and salinity gradients.
1656 *Journal of Geophysical Research: Oceans*, 121(2), 1229-1248.
1657 <https://doi.org/10.1002/2015JC011427>
- 1658 Wright, R. M., Le Quéré, C., Buitenhuis, E., Pitois, S., and Gibbons, M. J. (2021). Role of
1659 jellyfish in the plankton ecosystem revealed using a global ocean biogeochemical model.
1660 *Biogeosciences*, 18, 1291–1320, <https://doi.org/10.5194/bg-18-1291-2021>
- 1661 Zeng, J., Iida, Y., Matsunaga, T., & Shirai, T. (2022). Surface ocean CO₂ concentration and air-
1662 sea flux estimate by machine learning with modelled variable trends. *Frontiers in Marine*
1663 *Science*, 0-14. <https://doi.org/10.3389/fmars.2022.989233>
- 1664 Zunino, P., Pérez, F. F., Fajar, N. M., Guallart, E. F., Ríos, A. F., Pelegrí, J. L., & Hernández-
1665 Guerra, A. (2015). Transports and budgets of anthropogenic CO₂ in the tropical North Atlantic
1666 in 1992–1993 and 2010–2011. *Global Biogeochemical Cycles*, 29(7), 1075–1091.
1667 <https://doi.org/10.1002/2014GB005075>
- 1668
- 1669